

PREPARED FOR SUBMISSION TO JHEP

# Black Holes, Dark Matter Spikes, and Constraints on Simplified Models with $t$ -Channel Mediators

Pearl Sandick, Kuver Sinha, and Takahiro Yamamoto

*Department of Physics and Astronomy, University of Utah, Salt Lake City, UT 84112, USA*

*E-mail:* [sandick@physics.utah.edu](mailto:sandick@physics.utah.edu), [kuver.sinha@gmail.com](mailto:kuver.sinha@gmail.com),  
[t.yamamoto.1777@gmail.com](mailto:t.yamamoto.1777@gmail.com)

ABSTRACT:

The density spike of dark matter (DM) in the subparsec region near the supermassive black hole at the Galactic Center can provide potentially observable gamma-ray signals emanating from DM annihilations. Taking Fermi-*LAT* data for the gamma-ray flux from the point source 3FGL J1745.6-2859c (Sgr A\*), we calculate the resulting constraints on generic models of DM, allowing for the possibility of a non-negligible velocity-dependent component of the annihilation cross section. We consider a variety of selections for the astrophysical parameters that describe the spike profile and find that the gamma-ray flux is strongly dependent on these selections, particularly the modelling of spike depletion effects due to gravitational interactions with baryons, which affect the spike radius and steepness profile. We calculate constraints on the DM parameter space for different choices of spike radii, assuming an idealized case where no attenuation occurs, as well as a case where the spike is depleted. In each case we consider different choices for the steepness profiles. We find that for the most conservative selection of parameters, corresponding to a depleted spike with an NFW cusp profile, the gamma-ray flux for a 100 GeV thermal relic is lower than current observational constraints by several orders of magnitude. For more optimistic choices of parameters corresponding to spikes that have not been attenuated, bounds on DM masses can be obtained, which depend on the assumed steepness profiles. We give these bounds for a variety of choices of steepness profiles. We then specialize to a class of simplified models of fermionic DM that annihilate dominantly through the  $t$ -channel exchange of two scalar mediators with arbitrary mixing angle  $\alpha$ , and calculate the indirect detection constraints coming from the DM spike, in regions of parameter space that are complementary to collider searches. Along the way, we discuss constraints on the astrophysical parameters describing the DM spike, taking the Galactic Center excess as a signal of DM annihilation.

KEYWORDS: Dark Matter, Phenomenological Models, Simplified Models

---

## Contents

<b>1</b>	<b>Introduction</b>	<b>1</b>
<b>2</b>	<b>Dark Matter Spike Near the Supermassive Black Hole</b>	<b>3</b>
2.1	Spike Radius ( $r_{sp}$ )	4
2.2	Spike Profile	6
<b>3</b>	<b>Results</b>	<b>7</b>
<b>4</b>	<b>Constraints on Simplified Models</b>	<b>15</b>
4.1	Simplified Model with $t$ -channel Mediators	15
4.2	DM Annihilation	17
4.3	Results for Simplified Model	18
<b>5</b>	<b>Constraints on Spike Parameters from DM Annihilations</b>	<b>21</b>
<b>6</b>	<b>Conclusions</b>	<b>25</b>
<b>7</b>	<b>Acknowledgement</b>	<b>26</b>

---

## 1 Introduction

The particle nature of dark matter (DM) is an area of intense investigation which has the potential to shed light on fundamental questions about the Standard Model (SM), especially the hierarchy problem. For DM candidates with weak-scale couplings and mass, a calculation of the relic density automatically yields a value that is close to the measured relic abundance. This striking fact, success of the so-called Weakly Interacting Massive Particle (WIMP) paradigm, reinforces the possibility that DM is deeply connected to new physics at the weak scale. The indirect detection of the products of DM annihilation or decay have proven to be a particularly fruitful way to investigate the properties of DM.

Indirect detection of WIMPs in the Milky Way halo has been a major endeavor over many years. The gamma-ray flux  $\Phi$  coming from WIMP annihilation is proportional to the line-of-sight integral of the square of the DM density,

$$\Phi \sim \int \rho^2(r) dr . \quad (1.1)$$

Since the Galactic Center is expected to have a very high density of DM, it has been a much-studied source for indirect detection.

The formation of black holes at the centers of DM halos, and in particular the supermassive black hole at the center of our Galaxy [1, 2], can significantly modify the DM profile and affect the observed gamma-ray flux from that region. Gondolo and Silk showed [3] that if the black hole grows adiabatically at the center of a cusp with a power-law profile,

$$\rho(r) \sim r^{-\gamma_c} \quad (\text{cusp profile}), \quad (1.2)$$

a DM spike can form close to the black hole, with a density profile given by

$$\rho(r) \sim r^{-\gamma_{sp}} \quad (\text{spike profile}), \quad (1.3)$$

where  $\gamma_c$  and  $\gamma_{sp}$  may be related in specific ways that we discuss later. Such a spike causes  $\Phi$  to become large due to the diverging density  $\rho$  in Eq. 1.3 at small radii. This divergence is cut off by the black hole horizon and smoothed near it due to the effects of DM annihilation.

The account above is an idealized case, since the DM spike can be destroyed or smoothed by various effects [4–8]. In galactic nuclei, stars have much larger kinetic energy than DM particles, and interactions between them cause DM to be heated up. The gravitational interaction between stars near the black hole and the DM spike can thus cause damping, which affects the spike parameters, including the power-law behavior and the spike radius. The astrophysical parameters that describe the DM spike are a topic of ongoing debate, with several possibilities being plausible.

The purpose of this paper is to investigate contributions of Eq. 1.3 to the gamma-ray flux  $\Phi$ , taking into account different spike profiles and histories, and ultimately mapping them to models of DM with both velocity-dependent as well as velocity-independent contributions to the annihilation cross section. As our reference gamma-ray source, we take 3FGL J1745.6-2859c (Sgr A\*) from Fermi-*LAT*’s Third Point Source Catalog [9]. We consider cases where the DM profile is an idealized spike that has not suffered attenuation, as well as cases where gravitational interactions with baryons have caused the spike to be depleted. We thus consider the cases of an idealized and attenuated spike radius, respectively, as well as different power-law profiles, both outside and inside the spike radius. Finally, we specialize to a class of simplified models of fermionic DM that annihilate dominantly through the  $t$ -channel exchange of two scalar mediators with arbitrary mixing angle  $\alpha$ , and calculate the indirect detection constraints coming from the DM spike in this class of models.

Indirect detection of DM from a spike near the central black hole of our galaxy has been studied in the context of particle physics by several authors in different contexts. Recently, [10–12] have studied these issues for DM models with  $p$ -wave annihilation, as well as in the context of the Galactic Center excess. Indirect detection for models of DM with velocity-dependent annihilation cross section has been studied by [13], in models of non-thermal DM by [14], and in the context of dark stars by [15–17]. Spikes at the center of dwarf galaxies have recently been constrained by [18].

Our study takes into account the various possible histories of the DM spike near the central black hole of our galaxy. We find that the spike radius and the steepness profile both

inside and outside the spike radius have a have a strong effect on the resulting constraints on DM models. We consider several sets of parameter choices, corresponding to different histories. For convenience, we summarize our main results:

(i) The most conservative choice of parameters, corresponding to an attenuated spike radius, an NFW profile for the DM cusp  $\gamma_c = 1.0$ , and a flattened annihilation core yields a flux  $\Phi$  that is several orders of magnitude below the current observational threshold for a 100 GeV DM thermal relic (see the top left panel of Fig. 2).

(ii) For a less conservative choice of parameters, corresponding to an attenuated spike radius, but a selection of steeper profiles for the DM cusp  $\gamma_c = 1.1 - 1.5$ , thermal relics of various masses may be constrained as shown in Fig. 5. The constraints in the DM annihilation plane are plotted in the top right and bottom panels of Fig. 2 and Fig. 3.

(iii) Assuming that the spike has not undergone depletion improves the constraints considerably. In this idealized case, one can constrain thermal relics of different masses as shown in Fig. 6, which displays various choices of  $\gamma_c$ , and assumes the steepest inner spike profile  $\gamma_{sp}$ . This steepest choice corresponds to a spike formed by a collisionless DM halo assuming adiabatic growth of a central black hole.

(iv) In an idealized case where the spike has not undergone depletion, one can relax the assumption of the steepest inner profile and choose smaller values of  $\gamma_{sp}$ . The results are more conservative than Case (iii), and are displayed in Fig. 7.

Our work thus suggests that a more careful study of the astrophysics of DM spikes near black holes is warranted. The wide range of spike parameters can have a significant variation on the space of DM constraints. To illustrate this, we take the above cases and apply them to our simplified model, with results that are depicted in Fig. 9 - Fig. 13.

The paper is structured as follows. In Section 2, we discuss the parameters that describe the DM spike near the black hole. In Section 3, we discuss our main results in general DM models. In Section 4, we describe our results in the context of simplified DM models with  $t$ -channel mediators. In Section 5, we discuss the constraints on spike parameters coming from using the Galactic Center excess as a candidate of DM annihilation in a spike near the central massive black hole. We end with our Conclusions.

## 2 Dark Matter Spike Near the Supermassive Black Hole

In this section, we discuss the profile of a DM spike near the supermassive black hole (SMBH) in the inner subparsec region of our Galaxy. This has been studied by many groups, starting with the work of Gondolo and Silk [3].

Though we are agnostic about the nature of DM, we parametrize its annihilation cross section in the following standard way [? ]

$$\langle\sigma v\rangle\sim c_0+c_1\left(\frac{v}{c}\right)^2, \quad (2.1)$$

where  $c_0$  is the velocity-independent  $s$ -wave contribution, and  $c_1$  is the  $v^2$ -suppressed contribution. We note that the velocity-suppressed terms arise from both  $s$ -wave and  $p$ -wave matrix elements.

We consider a SMBH at the center of our Galaxy with mass  $M_{bh}$  and Schwarzschild radius  $r_{Sch.}$  [1]

$$\begin{aligned} M_{bh} &= 4 \times 10^6 M_\odot \\ r_{Sch.} &\sim 4 \times 10^{-7} \text{ pc} . \end{aligned} \quad (2.2)$$

The formation of a DM spike is contingent on several conditions, detailed for example in [3] and [4]. After its formation, the DM spike may be dampened due to gravitational interactions with the dense stellar core, or disrupted due to halo mergers which can substantially reduce the steepness of the spike. We will consider the case of a spike that has been depleted due to baryonic interactions, for which a simple parametrization has been provided in [8].

The profile is given in Fig. 1. We take the analytic form

$$\rho(r) = \begin{cases} \rho(r_{core}) & 10r_{Sch.} < r \leq r_{core} \\ \rho_0 (r/r_{sp})^{-\gamma_{sp}} & r_{core} < r \leq r_{sp} , \\ \rho_0 (r/r_{sp})^{-\gamma_c} & r_{sp} < r , \end{cases} \quad (2.3)$$

Here,  $r_{sp}$  and  $r_{core}$  denote the spike and core radii, respectively. The profile depends on the steepness parameters  $\gamma_{sp}$  and  $\gamma_c$ . We first give details about the spike and core radius, and then describe the steepness parameters for each region in the profile.

## 2.1 Spike Radius ( $r_{sp}$ )

In the idealized case, the spike radius is given as a function of time by

$$r_{sp}(t) = r_{sp}(0) \sim 0.2r_h \quad (\text{Idealized Case}). \quad (2.4)$$

Here,  $r_h$  denotes the radius of gravitational influence of the black hole, and is given by

$$r_h \equiv \frac{GM_{bh}}{\sigma^2} , \quad (2.5)$$

where  $G$  is Newton's constant and  $\sigma$  denotes the one-dimensional velocity dispersion.  $M_{bh}$  is related to  $\sigma$  through the empirical relation [24]

$$\frac{M_{bh}}{10^8 M_\odot} = (1.66 \pm 0.24) \left( \frac{\sigma}{200 \text{ km s}^{-1}} \right)^{4.86 \pm 0.43} . \quad (2.6)$$

For the central values in Eq. 2.6, we obtain

$$\begin{aligned} \sigma &\sim 93 \text{ km/s} \\ r_h &\sim 1.99 \text{ pc} \end{aligned} \quad (2.7)$$

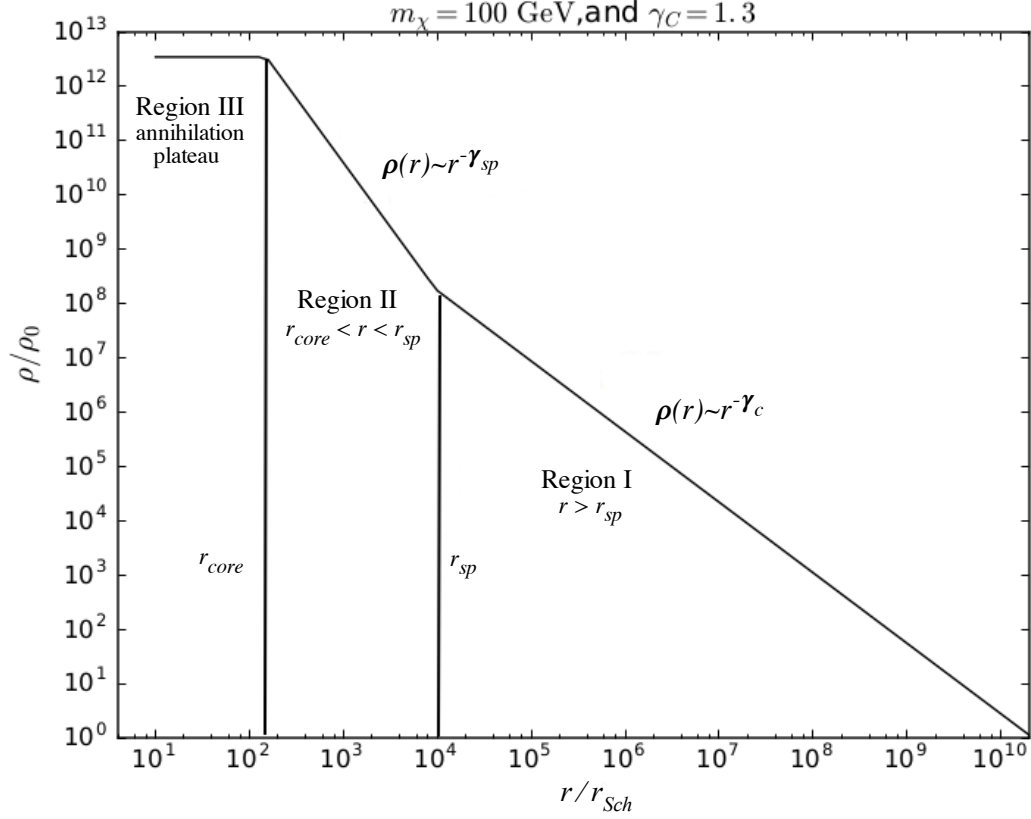


**Figure 1.** We display the DM profile for a typical choice of parameters  $\gamma_c = 1$ ,  $\gamma_{sp} = 7/3$ .

for the DM velocity dispersion and the radius of influence of the black hole. In the idealized case, this leads to a spike radius of

$$r_{sp} = 0.40 \text{ pc} \quad (\text{Idealized Case}). \quad (2.8)$$

Gravitational interactions between DM and baryons will lead to changes from the idealized case of Eq. 2.4. Stars in the galactic nucleus have much larger kinetic energy than DM, and the interactions between the two tend to heat up the DM. This leads to a dampening of the spike. The decay of the spike can be described roughly as

$$\rho(r, t) \approx \rho(r, 0) e^{-\tau/2}, \quad (2.9)$$

where  $\tau$  is the time since the spike formed, in units of the heating time,  $t_{\text{heat}}$  [8]. The heating time is  $t_{\text{heat}} \approx 10^9$  years, and we will take  $\tau = 10$  [23].

The evolution of the spike radius can then be described by the following expression [8]

$$\begin{aligned} r_{sp}(t) &= r_{sp}(0) \times \exp\left(\frac{-\tau}{2(\gamma_{sp} - \gamma_c)}\right) \\ \Rightarrow r_{sp}(t) &= 0.2r_h \times \exp\left(\frac{-\tau}{2(\gamma_{sp} - \gamma_c)}\right) \quad \textbf{(Depleted Case)} \end{aligned} \quad (2.10)$$

where  $r_{sp}(0)$  is the initial value,  $r_{sp}(0) = 0.2r_h$ . Typical values for the depleted spike radius are

$$\begin{aligned} r_{sp} &= 0.046 \text{ pc for } \gamma_c = 1.0 \\ r_{sp} &= 0.002 \text{ pc for } \gamma_c = 1.5 \quad \textbf{(Depleted Case)}, \end{aligned} \quad (2.11)$$

assuming a relation between  $\gamma_{sp}$  and  $\gamma_c$  as in Equation 2.16, described in Section 2.2. Note that the spike radius in the depleted case is much smaller than in the idealized case, and also that there is significant variation in the spike radius depending on  $\gamma_c$ . We consider both idealized and depleted spikes in our calculations going forward.

## 2.2 Spike Profile

In this section, we discuss the halo profile of the DM spike, starting from the outermost region and going to the innermost region.

**Region I - Outside the spike radius  $r_{sp}$ :** The growth of the DM spike starts from the inner halo, which for an NFW-like profile is given by

$$\rho(r) = \rho_0 \left(\frac{r}{r_{sp}}\right)^{-\gamma_c} \quad \text{for } r_{sp} < r. \quad (2.12)$$

The normalization of the density profile  $\rho_0$  has been set by extrapolating inwards from the solar radius

$$\rho_0 = \rho_\odot \left(\frac{r_\odot}{r_{sp}}\right)^{\gamma_c}. \quad (2.13)$$

Here, we take the density at the solar radius  $\rho_\odot = 0.3 \text{ GeV/cm}^3$ .

Simulations with only DM generally favor inner slope with  $\gamma_c \sim 1$ , which is the canonical NFW value. However, baryonic interactions affect the profile in the inner 10 kpc of our galaxy, and can substantially steepen the power-law behavior [25–29]. Since this is a matter of ongoing debate, we consider a range of DM profiles, keeping  $\gamma_c$  as a free parameter in a range acceptable in the current literature

$$\gamma_c = 1.0 - 1.5. \quad (2.14)$$

**Region II - Inside the spike radius  $r_{sp}$  but outside the core radius  $r_{core}$ :** The profile in this interval is

$$\rho(r) = \rho_0 \left(\frac{r}{r_{sp}}\right)^{-\gamma_{sp}} \quad \text{for } r_{core} < r < r_{sp}. \quad (2.15)$$

The spike slope can take a range of values. For collisionless DM forming a spike due to the adiabatic growth of the black hole, the spike parameter obeys the relation

$$\gamma_{sp} = \frac{9 - 2\gamma_c}{4 - \gamma_c} , \quad (2.16)$$

which yields a value  $\gamma_{sp} \approx 2.3 - 2.4$  for  $1.0 \leq \gamma_c \leq 1.5$ . This relation holds for a central black hole that grows adiabatically from a small seed. The spike slope can be different under different assumptions. If the black hole appeared instantaneously, then one obtains  $\gamma_{sp} = 4/3$  [4]. Black hole mergers at the center of the progenitor halo can give  $\gamma_{sp} = 1/2$ , a value that is also obtained if the black hole grows away from the center of the DM distribution. Taking into account stellar heating could result in a final equilibrium value as low as  $\gamma_{sp} \sim 1.5$ , or an intermediate value  $\gamma_{sp} \sim 1.8$  [10]. We will consider both the adiabatic case in Eq. 2.16, as well as an intermediate value  $\gamma_{sp} = 1.8$ .

**Region III - Inside the core radius  $r_{core}$ :** For small radii, the DM densities can reach very high values. But that also implies large values of the annihilation cross section, which acts to reduce the density. We will make the conservative assumption that an annihilation plateau is formed in this region, with

$$\rho(r) = \rho(r_{core}) \text{ for } 10r_{Sch.} < r < r_{core} , \quad (2.17)$$

where the lower limit is provided by the Schwarzschild radius of the black hole, and the upper limit corresponds to the core radius, which is defined by the relation

$$\frac{\rho(r_{core})}{m_\chi} \langle \sigma v \rangle \sim (\tau t_{\text{heat}})^{-1} , \quad (2.18)$$

which depends on the thermally averaged annihilation cross section times velocity,  $\langle \sigma v \rangle$ , and the WIMP mass,  $m_\chi$ .

We note that in the general case of arbitrary velocity anisotropy, instead of circular particle orbits, a cusp with  $\rho \sim r^{(-\beta-1/2)}$  may develop in the center, where  $\beta$  is the anisotropy coefficient [30]. This cusp may further enhance the flux. We will stay in the limit  $\beta \rightarrow -\infty$ , which corresponds to circular orbits.

### 3 Results

In this Section, we discuss our calculation of the gamma-ray flux. We first summarize all the input parameters from astrophysics as well as the DM simplified model.

We recall that the DM annihilation cross section has been parametrized in the following convenient way

$$\sigma v = c_0 + c_1 \left( \frac{v}{c} \right)^2 , \quad (3.1)$$

where  $v$  denotes the relative velocity of the DM particles. The core radius  $r_{core}$  is determined from Eq. 2.18. Assuming a virialized halo such that

$$\left( \frac{v}{c} \right)^2 = \frac{r_{Sch.}}{2r} , \quad (3.2)$$



and, combining Eq. 2.18 and Eq. 3.1, one can obtain the core radius  $r_{core}$  for different values of  $c_0$  and  $c_1$ .

The other spike parameters are given as follows:

(i) spike radius  $r_{sp}$  is given by Eq. 2.10.

(ii) the spike slopes  $\gamma_c$  and  $\gamma_{sp}$  are given by Eq. 2.14 and Eq. 2.16, respectively.

With these input parameters, we can now calculate the gamma-ray flux coming from DM annihilation. The differential flux of gamma rays from a given angular direction  $d\Omega$  produced by the annihilation of Majorana DM is given by

$$\frac{d\Phi_\gamma}{d\Omega dE} = \frac{1}{2} \frac{r_\odot}{4\pi} \left( \frac{\rho_\odot}{M_{DM}} \right)^2 \int_{l.o.s.} \frac{ds}{r_\odot} \left( \frac{\rho(r(s, \theta))}{\rho_\odot} \right)^2 \sum_f \langle \sigma v \rangle_f \frac{dN_\gamma^f}{dE}. \quad (3.3)$$

Here,  $r(s, \theta) = (r_\odot^2 + s^2 - 2r_\odot s \cos \theta)^{1/2}$ , and  $\theta$  is the aperture angle between the direction of the line of sight and the axis connecting the Earth to the Galactic Center.  $dN_\gamma^f/dE$  is the spectrum of photons coming from annihilation to a final state  $f$ , and is computed with Pythia [31]. We note that the usual separation between the  $J$ -factor and the annihilation cross section is no longer applicable here. This is because the annihilation cross section itself depends on position, from Eq. 3.2.

If the DM spike is a bright and compact enough source of photons, it may have been identified as a point source in Fermi-LAT's Third Point Source Catalog. We will thus be interested in computing the total flux from the DM spike and comparing the brightness to point sources in the same region. As a comparative value that determines observability, we consider the integrated flux from 1 to 100 GeV for the Fermi 3FGL source J1745.6-2859c (Sgr A\*), which we denote as  $\Phi_{Fermi} = 2.18 \times 10^{-8}$  photons/cm<sup>2</sup>s. In order to remain agnostic about the specific final states to which dark matter annihilates, we choose as a benchmark value for the integrated photon count  $N = 1$ , with the flux scaling  $\propto N$ .

The results are shown on the  $(c_0, c_1)$  planes in Fig. 2 and Fig. 3, for  $m_\chi = 100$  GeV and  $m_\chi = 200$  GeV, respectively. We choose a range of values of  $\gamma_c = 1.0, 1.3$ , and  $1.5$ . The contours show the total integrated flux  $\Phi$  in units of  $\Phi_{Fermi}$ . We see that for  $\gamma_c = 1.0$  and  $\gamma_c = 1.3$ , the total integrated flux  $\Phi$  is below current observational limits for  $c_0 \lesssim 10^{-25}$  cm<sup>3</sup> s<sup>-1</sup> and  $c_1 \lesssim 10^{-24}$  cm<sup>3</sup> s<sup>-1</sup>. For  $\gamma_c = 1.5$ , the observed gamma-ray flux constrains models with annihilation cross section  $c_0 \gtrsim 1.6 \times 10^{-26}$  cm<sup>3</sup> s<sup>-1</sup>. Therefore a canonical thermal relic with cross section  $3 \times 10^{-26}$  cm<sup>3</sup> s<sup>-1</sup> is excluded by this choice of spike parameters if its mass  $s \lesssim 100$  GeV, though the constraints are weaker for heavier WIMPs.

Finally, we note that if the velocity-dependent component  $c_1$  provides the dominant contribution to the photon flux, it must be significantly larger than  $c_0$  need be if it dominates. This is due to the factor  $(v/c)^2 \sim (r_{Sch.}/2r)$ , which is small away from the central black hole.

In Fig. 4, we show contours of the ratio  $\Phi/\Phi_{NFW}$ , where  $\Phi$  and  $\Phi_{NFW}$  are the total integrated flux in the presence and absence (i.e. standard NFW profile), respectively, of a DM spike near the supermassive black hole. The spike power law outside the spike radius is given by  $\gamma_c = 1.5$  and law inside the spike radius is given by Eq. 2.16. The DM mass is 100



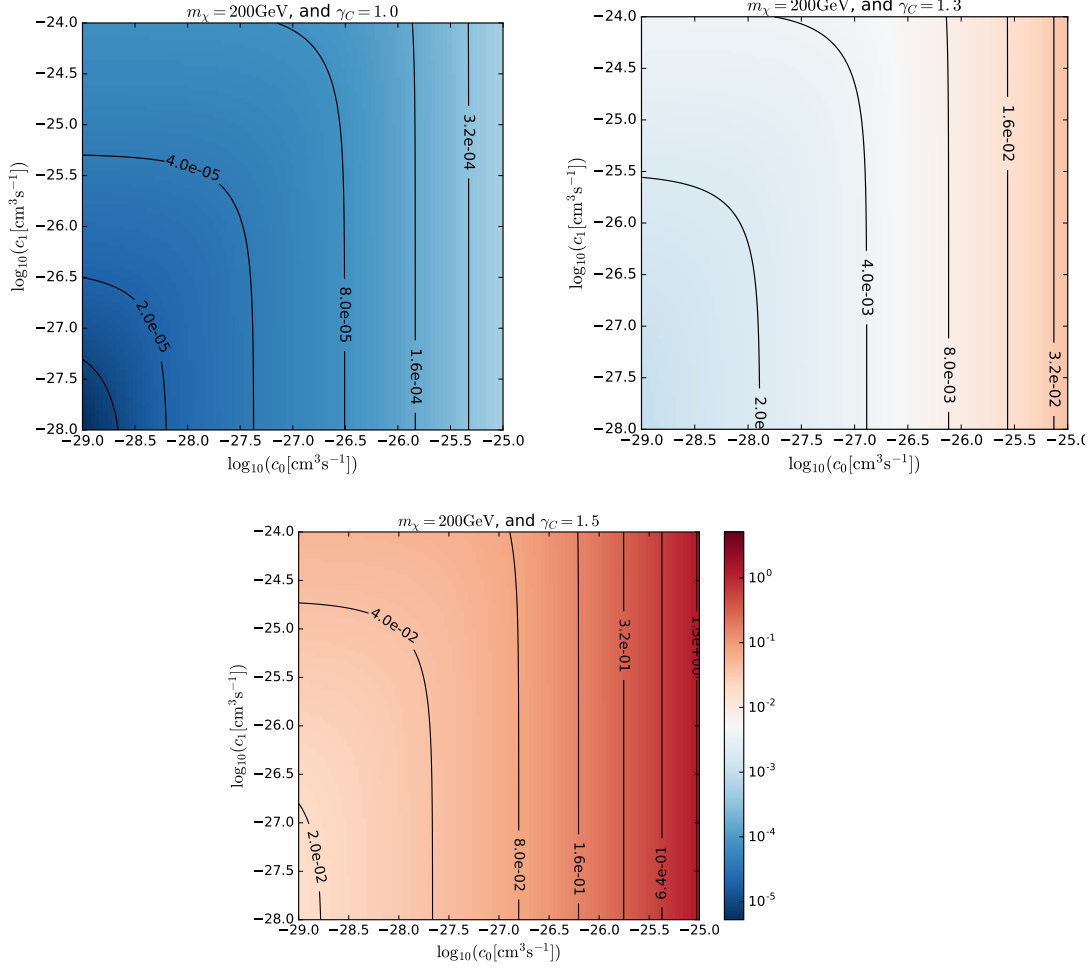


**Figure 3. Depleted Spike, 200 GeV DM: Contours of the integrated flux  $\Phi$**  in units of  $\Phi_{Fermi} = 2.18 \times 10^{-8}$  photons/cm<sup>2</sup>s coming from the source 3FGL J1745.6-2859c (Sgr A\*), in the energy range 1-100 GeV, and assuming an integrated photon count  $N = 1$ . The dark matter mass is 200 GeV, and the annihilation cross section is parametrized by Eq. 3.1. The spike profile is given by Eq. 2.3. The spike radius is given by the depleted case in Eq. 2.10, with values  $r_{sp} \sim 0.002 - 0.046$  pc. The spike power law outside the spike radius is given by  $\gamma_c = 1.0$  (upper left panel),  $\gamma_c = 1.3$  (upper right panel), and  $\gamma_c = 1.5$  (lower panel). The spike power law inside the spike radius is given by Eq. 2.16, yielding values in the range  $\gamma_{sp} \sim 2.3 - 2.4$ .

spike radius is given by Eq. 2.16. The contours are the total integrated flux  $\Phi$  in units of  $\Phi_{Fermi} = 2.18 \times 10^{-8}$  photons/cm<sup>2</sup>s in the energy range 1-100 GeV and a benchmark integrated photon count  $N = 1$ . The annihilation cross section is parametrized by Eq. 3.1, with  $c_0 = 3 \times 10^{-26}$  cm<sup>3</sup> s<sup>-1</sup> and  $c_1 = 1 \times 10^{-30}$  cm<sup>3</sup> s<sup>-1</sup>, corresponding to a canonical thermal relic. The dashed line shows the observational limit  $\Phi = \Phi_{Fermi}$ . From bottom to top, the cyan, blue, and magenta contours correspond to  $\gamma_c = 1.3$ ,  $\gamma_c = 1.4$ , and  $\gamma_c = 1.5$ , respectively.

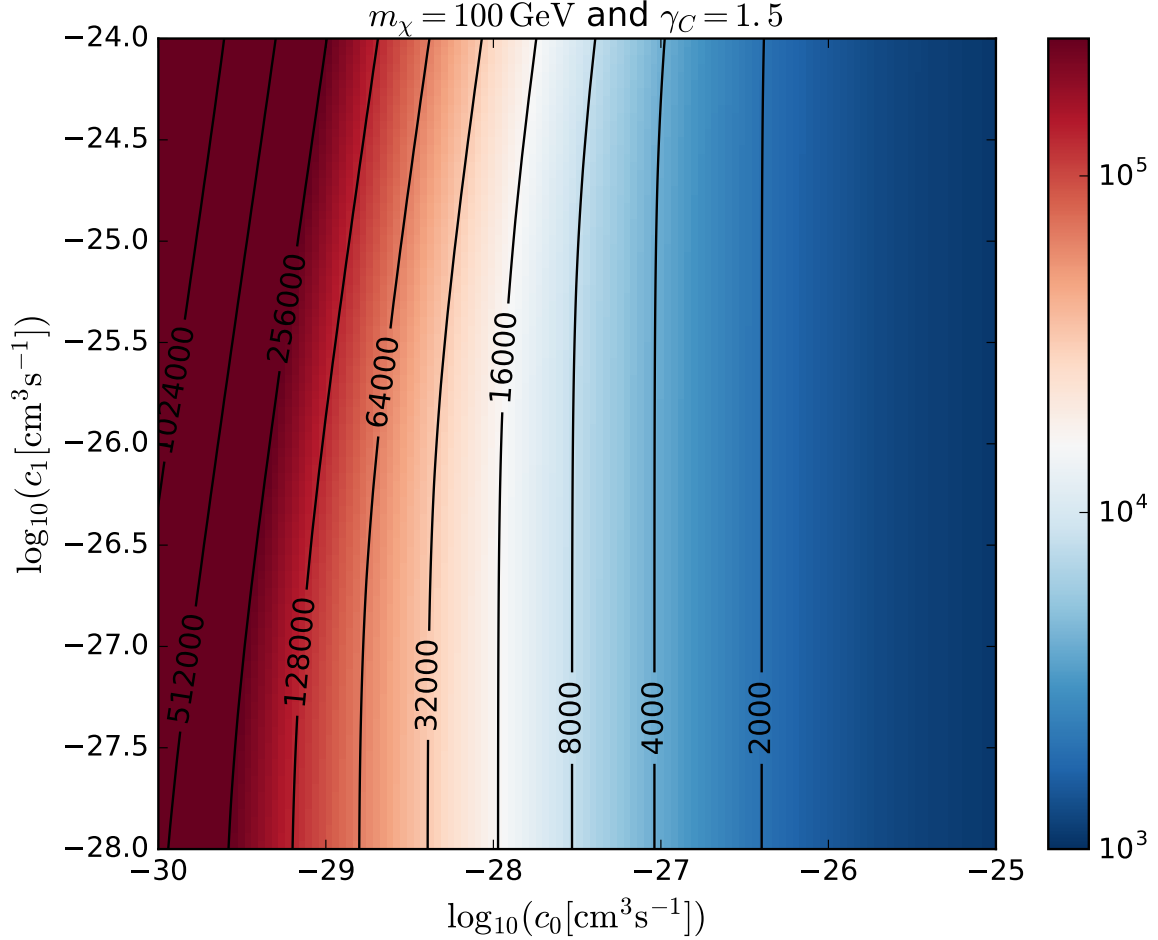


**Figure 4. Depleted Spike, Contours of the ratio  $\Phi/\Phi_{\text{NFW}}$** , where  $\Phi$  and  $\Phi_{\text{NFW}}$  are the total integrated flux in the presence and absence, respectively, of a DM spike near the supermassive black hole, coming from the source 3FGL J1745.6-2859c (Sgr A\*), in the energy range 1-100 GeV, and assuming an integrated photon count  $N = 1$ . The dark matter mass is 100 GeV, and the annihilation cross section is parametrized by Eq. 3.1. The spike profile is given by Eq. 2.3. The spike radius is given by the depleted case in Eq. 2.10, with value  $r_{sp} \sim 0.002$  pc. The spike power law outside the spike radius is given by  $\gamma_c = 1.5$ . The spike power law inside the spike radius is given by Eq. 2.16, with value  $\gamma_{sp} \sim 2.4$ .

We see that thermal relics with masses  $\lesssim 15$  GeV,  $\lesssim 50$  GeV, and  $\lesssim 140$  GeV, are constrained for depleted spikes with  $\gamma_c = 1.3, 1.4$ , and  $1.5$ , respectively and  $\gamma_{sp} = \frac{9-2\gamma_c}{4-\gamma_c}$ . Larger values of  $\gamma_c$  lead to steeper spike profiles both inside and outside the spike radius  $r_{sp}$ , leading to an increased integrated flux and stronger mass reach.

In Fig. 6, we show the observational limit as a function of the DM mass for the case of an idealized spike with spike radius given by Eq. 2.8. The spike power law inside the

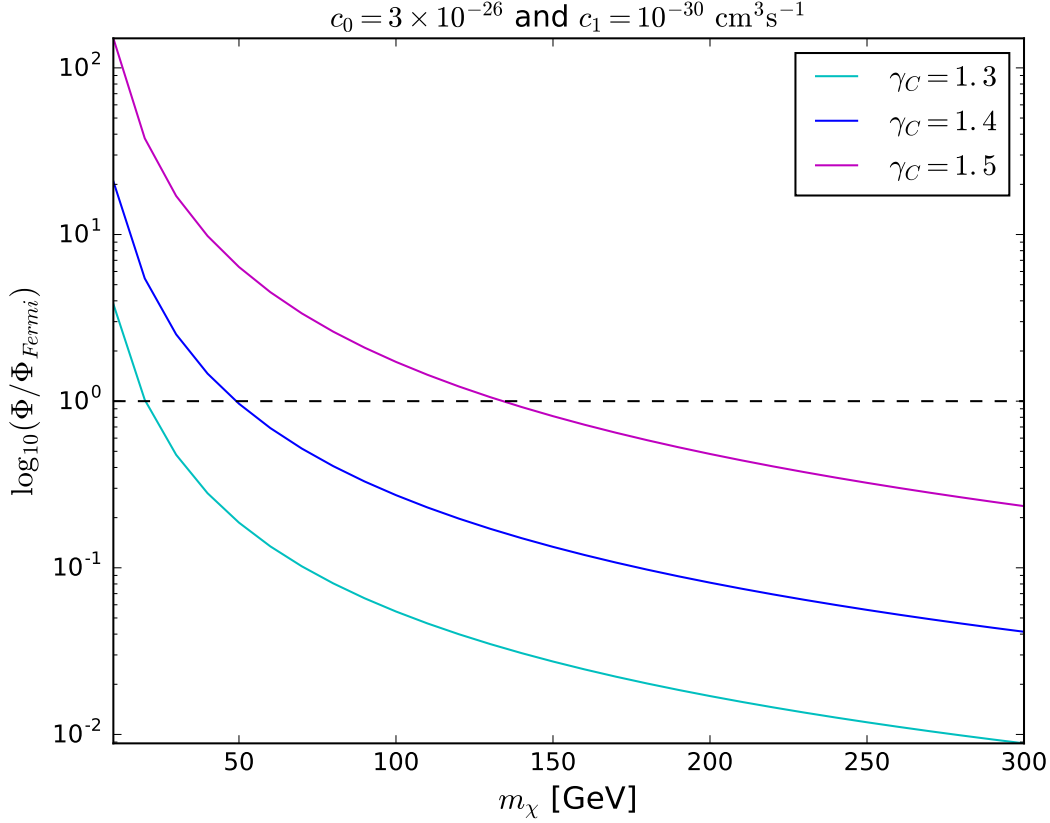


**Figure 5. Depleted spike with  $\gamma_{sp} = \frac{9-2\gamma_c}{4-\gamma_c} \sim 2.3 - 2.4$  : Observational reach versus mass plot** - The total integrated flux  $\Phi$  in units of  $\Phi_{Fermi} = 2.18 \times 10^{-8}$  photons/cm<sup>2</sup>s coming from the source 3FGL J1745.6-2859c (Sgr A\*), in the energy range 1-100 GeV, and assuming an integrated photon count  $N = 1$ . The annihilation cross section is parametrized by Eq. 3.1, with  $c_0 = 3 \times 10^{-26}$  cm<sup>3</sup> s<sup>-1</sup> and  $c_1 = 1 \times 10^{-30}$  cm<sup>3</sup> s<sup>-1</sup>, corresponding to a canonical thermal relic. The spike profile is given by Eq. 2.3. The spike radius is given by the depleted case in Eq. 2.10, with values  $r_{sp} \sim 0.002 - 0.046$  pc. The spike power law inside the spike radius is given by Eq. 2.16, yielding values in the range  $\gamma_{sp} \sim 2.3 - 2.4$ . The dotted line shows the observational limit  $\Phi = \Phi_{Fermi}$ . The cyan, blue, and magenta contours correspond to  $\gamma_c = 1.3$ ,  $\gamma_c = 1.4$ , and  $\gamma_c = 1.5$ , respectively.

spike radius is given by Eq. 2.16. The contours are the total integrated flux  $\Phi$  in units of  $\Phi_{Fermi} = 2.18 \times 10^{-8}$  photons/cm<sup>2</sup>s in the energy range 1-100 GeV and an integrated photon count  $N = 1$ . The annihilation cross section is parametrized by Eq. 3.1, with  $c_0 = 3 \times 10^{-26}$  cm<sup>3</sup> s<sup>-1</sup> and  $c_1 = 1 \times 10^{-30}$  cm<sup>3</sup> s<sup>-1</sup>, corresponding to a canonical thermal relic. The dotted line shows the observational limit  $\Phi = \Phi_{Fermi}$ . From bottom to top, the black, red, green, cyan, blue, and magenta contours correspond to  $\gamma_c = 1.0$ ,  $\gamma_c = 1.1$ ,  $\gamma_c = 1.2$ ,  $\gamma_c = 1.3$ ,  $\gamma_c = 1.4$ , and  $\gamma_c = 1.5$ , respectively.

We see that thermal relics with masses  $\lesssim 25$  GeV,  $\lesssim 80$  GeV, and  $\lesssim 240$  GeV are excluded

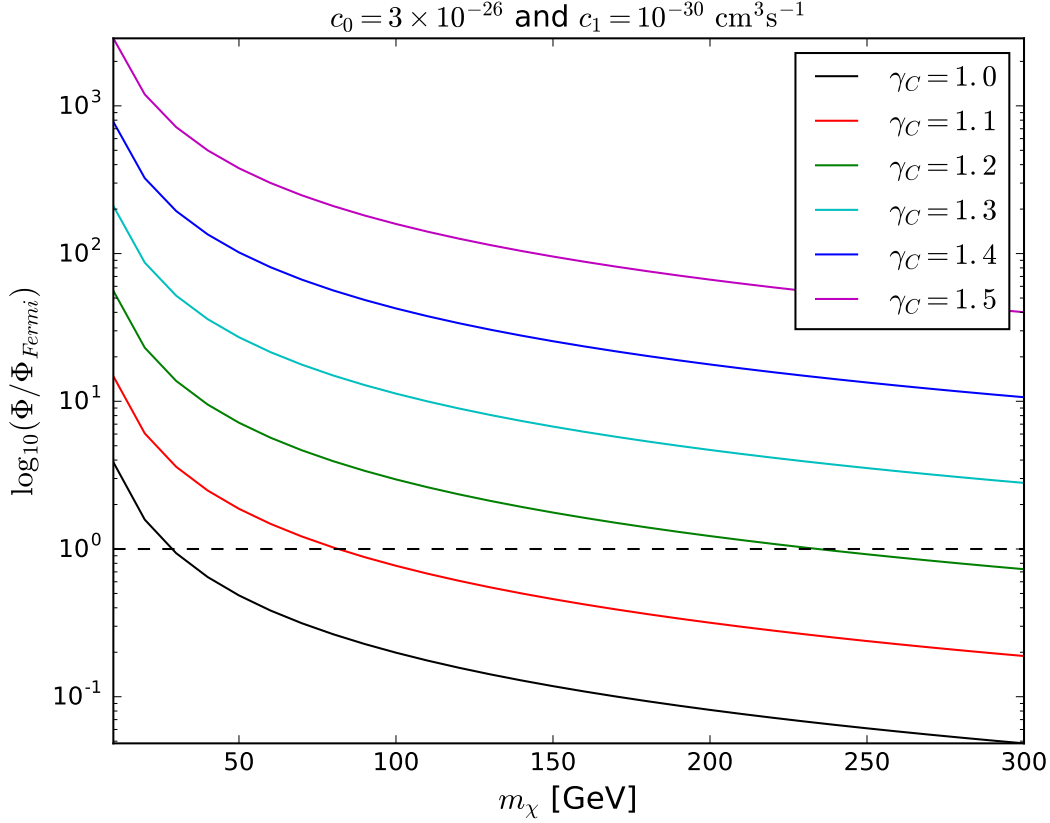


**Figure 6. Idealized spike with  $\gamma_{sp} = \frac{9-2\gamma_c}{4-\gamma_c}$  : Observational reach versus mass plot -** The total integrated flux  $\Phi$  in units of  $\Phi_{Fermi} = 2.18 \times 10^{-8}$  photons/cm<sup>2</sup>s coming from the source 3FGL J1745.6-2859c (Sgr A\*), in the energy range 1-100 GeV, and assuming an integrated photon count  $N = 1$ . The annihilation cross section is parametrized by Eq. 3.1, with  $c_0 = 3 \times 10^{-26}$  cm<sup>3</sup> s<sup>-1</sup> and  $c_1 = 1 \times 10^{-30}$  cm<sup>3</sup> s<sup>-1</sup>, corresponding to a canonical thermal relic. The spike profile is given by Eq. 2.3. The spike radius is given by the idealized case in Eq. 2.8, with value  $r_{sp} \sim 0.40$  pc. The spike power law inside the spike radius is given by Eq. 2.16, yielding values in the range  $\gamma_{sp} \sim 2.3 - 2.4$ . The dotted line shows the observational limit  $\Phi = \Phi_{Fermi}$ . The black, red, green, cyan, blue, and magenta contours correspond to  $\gamma_c = 1.0$ ,  $\gamma_c = 1.1$ ,  $\gamma_c = 1.2$ ,  $\gamma_c = 1.3$ ,  $\gamma_c = 1.4$ , and  $\gamma_c = 1.5$ , respectively.

for idealized spikes with  $\gamma_c = 1.0$ , 1.1, and 1.2, respectively, and  $\gamma_{sp} = \frac{9-2\gamma_c}{4-\gamma_c}$ . Larger mass reach is possible for larger values of  $\gamma_c$ . The mass reach here is clearly much higher than in the case of a depleted spike.

In Fig. 7, we show the observational limit as a function of the DM mass for the case of an idealized spike with spike radius given by Eq. 2.8, but with  $\gamma_{sp} = 1.8$ . Other parameter choices are identical to Fig. 6. We see that thermal relics with masses  $\lesssim 15$  GeV,  $\lesssim 50$  GeV, and  $\lesssim 140$  GeV are constrained for idealized spikes with  $\gamma_c = 1.2$ , 1.3, and 1.4, respectively, for  $\gamma_{sp} = 1.8$ . Again, Larger mass reach is possible for larger values of  $\gamma_c$  but the mass reach

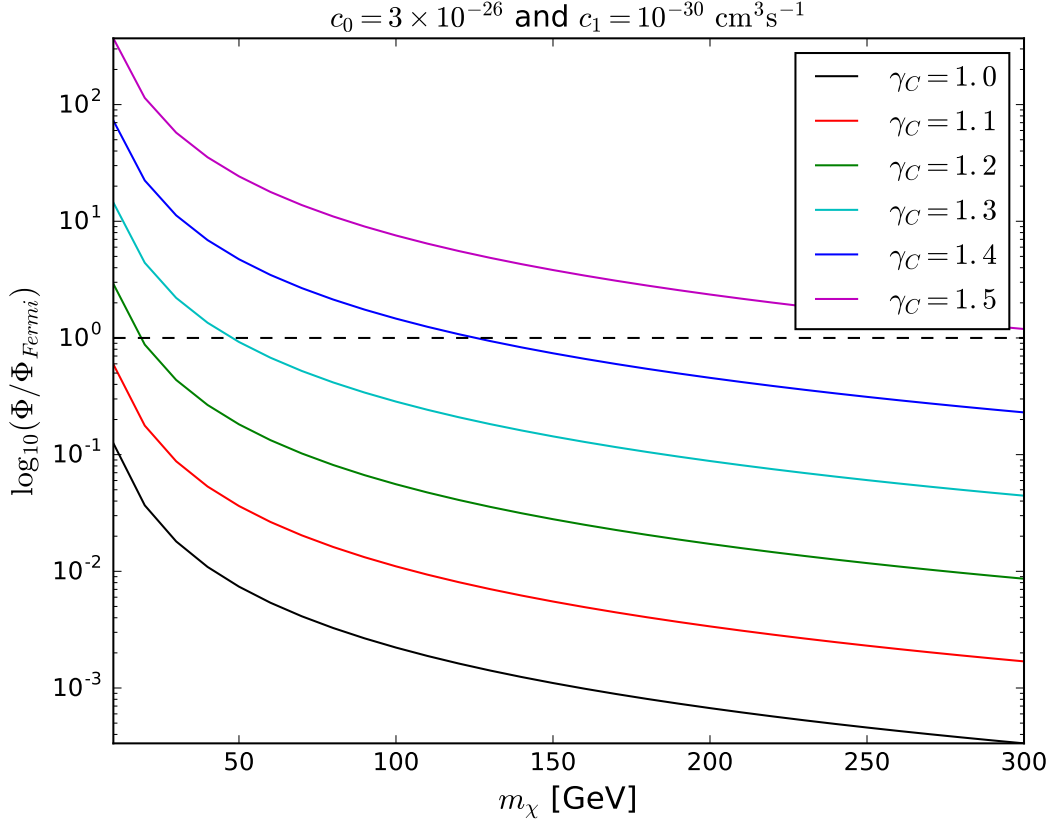


**Figure 7. Idealized spike with  $\gamma_{sp} = 1.8$  : Observational reach versus mass plot** - The total integrated flux  $\Phi$  in units of  $\Phi_{Fermi} = 2.18 \times 10^{-8}$  photons/cm<sup>2</sup>s coming from the source 3FGL J1745.6-2859c (Sgr A\*), in the energy range 1-100 GeV, and assuming an integrated photon count  $N = 1$ . The annihilation cross section is parametrized by Eq. 3.1, with  $c_0 = 3 \times 10^{-26}$  cm<sup>3</sup> s<sup>-1</sup> and  $c_1 = 1 \times 10^{-30}$  cm<sup>3</sup> s<sup>-1</sup>, corresponding to a canonical thermal relic. The spike profile is given by Eq. 2.3. The spike radius is given by the idealized case in Eq. 2.8, with value  $r_{sp} \sim 0.40$  pc. The spike power law inside the spike radius is given by  $\gamma_{sp} = 1.8$ . The dotted line shows the observational limit  $\Phi = \Phi_{Fermi}$ . The black, red, green, cyan, blue, and magenta contours correspond to  $\gamma_c = 1.0$ ,  $\gamma_c = 1.1$ ,  $\gamma_c = 1.2$ ,  $\gamma_c = 1.3$ ,  $\gamma_c = 1.4$ , and  $\gamma_c = 1.5$ , respectively.

here is clearly much lower than in Fig. 6 due to the smaller value of  $\gamma_{sp}$ .

Our results from this Section may be summarized as follows.=: The degree to which the DM spike near the black hole can constrain DM models depends strongly on the selection of parameters that determine the spike profile, such as the spike radius  $r_{sp}$  and the parameters  $\gamma_{sp}$  and  $\gamma_c$  describing the profile power-law behaviour inside and outside the spike radius, respectively. Different choices of these parameters have been considered, ranked in order from the most conservative to the most optimistic:

- (i) A depleted spike with radius given by Eq. 2.10,  $\gamma_c = 1.0$ , and  $\gamma_{sp}$  given by Eq. 2.16

( $\gamma_{sp} = \frac{9-2\gamma_c}{4-\gamma_c}$ ). This is the most conservative choice of parameters we study, and the results are shown in the top left panels of Fig. 2 and Fig. 3, for 100 GeV and 200 GeV DM, respectively. We see that for a 100 GeV DM candidate with annihilation cross section compatible with a thermal relic, this choice of spike parameters leads to a flux that is several orders of magnitude smaller than the current observational limit  $\Phi_{Fermi}$ . Smaller values of  $\gamma_{sp}$  would therefore also lead to unobservably small photon fluxes.

(ii) A depleted spike with radius given by Eq. 2.10,  $\gamma_c = 1.1 - 1.5$ , and  $\gamma_{sp}$  given by Eq. 2.16. The mass reaches are plotted in Fig. 5, and the constraints in the DM annihilation plane  $c_0$  and  $c_1$  are plotted in the top right and bottom panels of Fig. 2 and Fig. 3. It is clear that with increasing  $\gamma_c$ , the current observational limit  $\Phi_{Fermi}$  can put some constraints on DM of various masses.

(iii) An idealized spike with radius given by Eq. 2.4,  $\gamma_c = 1.0 - 1.5$ , and  $\gamma_{sp} = 1.8$ . The mass reaches are plotted in Fig. 7. Due to the larger spike radius, the reaches are generally greater than the depleted spike of Case (ii), even with the smaller value of  $\gamma_{sp}$ .

(iv) An idealized spike with radius given by Eq. 2.4,  $\gamma_c = 1.0 - 1.5$ , and  $\gamma_{sp} = \frac{9-2\gamma_c}{4-\gamma_c}$ . This is the most optimistic choice of parameters, and the results are shown in Fig. 6.

In particular, it is clear that for a given value DM mass and  $\gamma_{sp}$ , a comparison between the depleted spike in Case (i) and the idealized spike in Case (iv) shows that the flux increases by a factor of  $\sim \mathcal{O}(10^3)$  when one assumes that the spike radius remained at its idealized value. A comparison between Case (iii) and Case (iv) shows that for a given spike radius and DM mass, changing  $\gamma_{sp}$  from 1.8 to the value predicted from Eq. 2.16 (typically 2.3 – 2.4) increases the flux by  $\sim \mathcal{O}(10 - 10^2)$ .

## 4 Constraints on Simplified Models

In this Section, we describe the constraints that are obtained on simplified models of DM with  $t$ -channel mediators. For concreteness, we take the DM mass to be 100 GeV, with the spike profile, flux source, and energy threshold the same as in the general situation considered in Section 3. As an example, we consider DM annihilating to  $b\bar{b}$  final states.

We first describe this class of simplified models, and then provide a discussion of the results.

### 4.1 Simplified Model with $t$ -channel Mediators

In this section, we describe some general features of models of DM that annihilate primarily through the  $t$ -channel. There is a vast amount of literature on these models, and we refer the reader to [19] and references therein.

For simplicity, we focus on Majorana DM candidates  $\chi$  with mass  $m_\chi$  that couple to both left and right SM fermions  $f_{L,R}$ . The mediator sector consists of a pair of scalars  $\tilde{f}_{L,R}$ , with a mixing angle  $\alpha$  [20], [21]. The standard case of mediator sectors coupling to right-handed SM fermions corresponds to the choice  $\alpha = \pi/2$ .



The interaction Lagrangian is given by

$$\mathcal{L}_{\text{int}} = \lambda_L \tilde{f}_L^* \bar{\chi} P_L f + \lambda_R \tilde{f}_R^* \bar{\chi} P_R f + \text{c.c.} , \quad (4.1)$$

where the Yukawa couplings  $\lambda_{L,R}$  may in general contain a  $CP$ -violating phase,

$$\lambda_L \equiv |\lambda_L| e^{i\varphi/2} , \quad \lambda_R \equiv |\lambda_R| e^{-i\varphi/2} . \quad (4.2)$$

The mixing angle  $\alpha$  between the scalar mass and chiral eigenstates is given as follows

$$\begin{pmatrix} \tilde{f}_1 \\ \tilde{f}_2 \end{pmatrix} = \begin{pmatrix} \cos \alpha & -\sin \alpha \\ \sin \alpha & \cos \alpha \end{pmatrix} \begin{pmatrix} \tilde{f}_L \\ \tilde{f}_R \end{pmatrix} . \quad (4.3)$$

The two scalar mass eigenvalues are denoted as  $m_{\tilde{f}_1}$  and  $m_{\tilde{f}_2}$  in the following. There are thus the following free parameters in this class of simplified models [22]:

- the four masses  $m_\chi$ ,  $m_{\tilde{f}_1}$ ,  $m_{\tilde{f}_2}$  and  $m_f$ .
- the Yukawas  $|\lambda_{L,R}|$ , the  $CP$ -violation phase  $\varphi$ , and the scalar mixing angle  $\alpha$ .

The supersymmetric limit of our simplified model is obtained as follows: In the Minimal Supersymmetric Standard Model (MSSM), bino DM couples to one generation of light squarks or sleptons. The Yukawa couplings are given by

$$\begin{aligned} |\lambda_L| &= \sqrt{2}g|Y_L| \\ |\lambda_R| &= \sqrt{2}g|Y_R| , \end{aligned} \quad (4.4)$$

where  $g$  is the electroweak coupling constant. For leptons,  $|Y_L| = 1/2$  and  $|Y_R| = 1$ ; for quarks,  $|Y_L| = 1/3$  and  $|Y_R| = 2/3$ . The mass squared matrix of the slepton in the chiral basis is

$$-\mathcal{L} = \begin{pmatrix} \tilde{f}_L^* & \tilde{f}_R^* \end{pmatrix} \begin{pmatrix} m_{\tilde{f}_L}^2 & m_{\tilde{f}_{LR}}^2 \\ m_{\tilde{f}_{LR}}^2 & m_{\tilde{f}_R}^2 \end{pmatrix} \begin{pmatrix} \tilde{f}_L \\ \tilde{f}_R \end{pmatrix} . \quad (4.5)$$

The matrix entries are given by:

$$m_{\tilde{f}_L}^2 = m_{\tilde{L}}^2 + m_Z^2 \cos 2\beta (-1/2 + \sin^2 \theta_w) + m_f^2 , \quad (4.6a)$$

$$m_{\tilde{f}_R}^2 = m_{\tilde{E}}^2 - m_Z^2 \cos 2\beta \sin^2 \theta_w + m_f^2 , \quad (4.6b)$$

$$m_{\tilde{f}_{LR}}^2 = m_f (A_f - \mu \tan \beta) . \quad (4.6c)$$

The mixing angle  $\alpha$  is:

$$\sin \alpha = \frac{m_{\tilde{f}_{LR}}^2}{\sqrt{(m_{\tilde{f}_2}^2 - m_{\tilde{f}_L}^2)^2 + (m_{\tilde{f}_{LR}}^2)^2}} , \quad (4.7a)$$

$$\cos \alpha = \frac{m_{\tilde{f}_2}^2 - m_{\tilde{f}_L}^2}{\sqrt{(m_{\tilde{f}_2}^2 - m_{\tilde{f}_L}^2)^2 + (m_{\tilde{f}_{LR}}^2)^2}} , \quad (4.7b)$$

which leads to

$$\tan \alpha = \frac{m_f(A_f - \mu \tan \beta)}{m_{f_2}^2 - m_{f_L}^2}, \quad (4.7c)$$

## 4.2 DM Annihilation

We now discuss the annihilation channels of the DM  $\chi$ . The relevant diagrams are given in Fig. 8. Parametrizing the annihilation cross section in the standard way, the velocity-

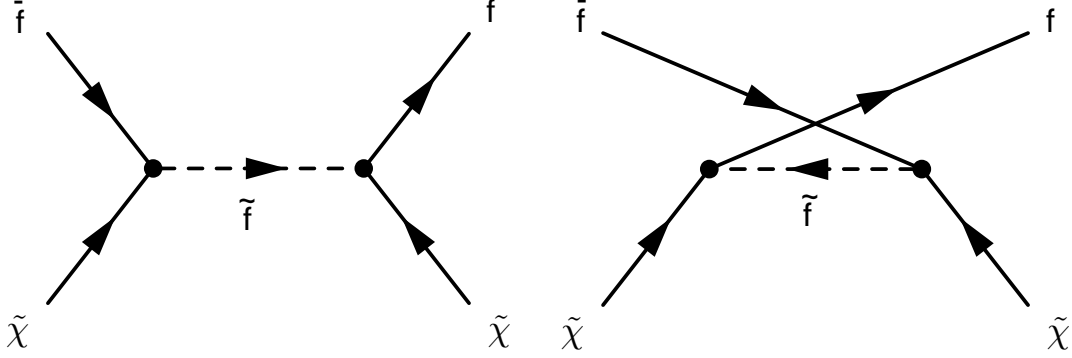


**Figure 8.** Feynman diagrams for DM annihilation in the  $t$ -channel.

independent  $s$ -wave contribution  $c_0$  is given in the limit  $m_f/m_{f_i} \rightarrow 0$  by the simple expression

$$c_0 = \frac{m_{\tilde{\chi}}^2}{2\pi} g^4 Y_L^2 Y_R^2 \cos^2 \alpha \sin^2 \alpha \left( \frac{1}{m_{f_1}^2 + m_{\tilde{\chi}}^2} - \frac{1}{m_{f_2}^2 + m_{\tilde{\chi}}^2} \right)^2, \quad (4.8)$$

In the limit  $m_f/m_{f_i} \rightarrow 0$ , the  $v^2$ -suppressed contribution,  $c_1$  simplifies considerably, and the analytic expression is

$$c_1 = \frac{m_{\tilde{\chi}}^2}{2\pi} g^4 \left( \frac{(Y_L^4 \cos^4 \alpha + Y_R^4 \sin^4 \alpha)(m_{f_1}^4 + m_{\tilde{\chi}}^4)}{(m_{f_1}^2 + m_{\tilde{\chi}}^2)^4} + \frac{(Y_L^4 \sin^4 \alpha + Y_R^4 \cos^4 \alpha)(m_{f_2}^4 + m_{\tilde{\chi}}^4)}{(m_{f_2}^2 + m_{\tilde{\chi}}^2)^4} \right. \\ + \frac{2(Y_L^4 + Y_R^4) \sin^2 \alpha \cos^2 \alpha (m_{f_1}^2 m_{f_2}^2 + m_{\tilde{\chi}}^4)}{(m_{f_1}^2 + m_{\tilde{\chi}}^2)^2 (m_{f_2}^2 + m_{\tilde{\chi}}^2)^2} \\ + \frac{Y_L^2 Y_R^2 \sin^2 \alpha \cos^2 \alpha (m_{f_1}^2 - m_{f_2}^2)^2}{2(m_{f_1}^2 + m_{\tilde{\chi}}^2)^4 (m_{f_2}^2 + m_{\tilde{\chi}}^2)^4} \left[ 3m_{f_1}^4 m_{f_2}^4 - 52m_{\tilde{\chi}}^4 m_{f_1}^2 m_{f_2}^2 + 3m_{\tilde{\chi}}^8 \right. \\ \left. \left. - 14m_{\tilde{\chi}}^2 (m_{f_1}^2 + m_{f_2}^2)(m_{\tilde{\chi}}^4 + m_{f_1}^2 m_{f_2}^2) - 5m_{\tilde{\chi}}^4 (m_{f_1}^4 + m_{f_2}^4) \right] \right). \quad (4.9)$$

We note that the velocity-suppressed terms arise from both  $s$ -wave and  $p$ -wave matrix elements. We also note that  $c_0$  and  $c_1$  do depend on  $\varphi$  in terms proportional to  $m_f$ . Additionally,

these  $m_f$ -dependent terms carry coefficients involving  $Y_L$  and  $Y_R$  such that there can be interesting cancellations, even in  $c_0$ . In our results, we will use the full expressions for  $c_0$  and  $c_1$ , including  $m_f$ -dependent terms.

### 4.3 Results for Simplified Model

We now discuss the constraints in the context of the simplified model discussed thus far. We adapt Fig. 2, which gave the contours of flux  $\Phi$  in units of the current observational limit  $\Phi_{Fermi}$  on the plane  $c_0$  vs.  $c_1$ , and scan over our simplified model on the same plane. We consider two representative cases: the case of a depleted spike with  $\gamma_c = 1.3$ , and the case of an idealized spike with  $\gamma_c = 1.0$ . For each case, we scan over the mixing angle  $\alpha$  and the Yukawa couplings of the simplified model.

In Fig. 9 and Fig. 10, we consider the case of a depleted spike and idealized spike, respectively. The green dots show a scan over the mixing angle  $\alpha$  defined by Eq. 4.3, holding the Yukawa couplings fixed at their supersymmetric values given in Eq. 4.4. The scan is performed in the range  $\alpha = 0$  to  $\pi/2$ . The low-energy spectrum of the SUSY model we consider consists of bino DM with mass  $m_\chi = 100$  GeV, the lightest bottom squark with mass  $m_{\tilde{b}} = 105$  GeV, and all other superpartners heavy. The solid black line denotes the contour of the integrated flux  $\Phi_{Fermi} = 2.18 \times 10^{-8}$  photons/cm<sup>2</sup>s.

From the depleted case with  $\gamma_c = 1.3$  considered in Fig. 9, we can see that current observational constraints just barely begin to constrain the parameter space. For  $\gamma_c = 1.0$ , the results are even weaker, while we have checked that the case of  $\gamma_c = 1.5$  constrains a significant portion of the parameter space. The constraints are much stronger for the case of an idealized spike in Fig. 10. We can see that even for  $\gamma_c = 1.0$  in the case of an idealized spike, the current observational limits constrain a large part of the parameter space.

The resulting constraints on  $\alpha$  are displayed in Fig. 11. The purple and blue curves show the dependence of  $c_0$  and  $c_1$  on  $\alpha$  as obtained from Eq. 4.8 and Eq. 4.9, respectively. For  $\alpha \approx 0, \pi/2$ , the annihilation cross section drops precipitously since the contribution from  $c_0$  suffers from chiral suppression and the contribution from  $c_1$  is velocity-suppressed. These are the regions where the scan in Fig. 10 is cut off towards the left, where  $c_0$  becomes small. Conversely, there is a range of values  $\alpha \approx 0.08\pi - 0.25\pi$ , where  $c_1$  becomes small, but  $c_0$  remains large. These are the regions that are cut off towards the bottom of the scan in Fig. 10, where  $c_1$  is small.

The horizontal dotted line in Fig. 11 corresponds to  $c_0 \approx 10^{-27} \text{ cm}^3 \text{ s}^{-1}$ , which is where the  $\Phi = \Phi_{Fermi}$  contour in Fig. 10 intersects the  $c_0$  axis. Values of  $c_0$  larger than this yield an integrated photon flux that is constrained by the source 3FGL J1745.6-2859c (Sgr A\*). Thus, from Fig. 11, it is clear that values of

$$0.04\pi \lesssim \alpha \lesssim 0.46\pi \quad (4.10)$$

are constrained by the gamma-ray flux.

In Fig. 12 and Fig. 13, we show a scan over the Yukawa couplings  $\lambda_{L,R}$  in the range 0 to  $\sqrt{4\pi}$ , for a fixed value of  $\alpha = \pi/4$ . The low-energy spectrum of the SUSY model we

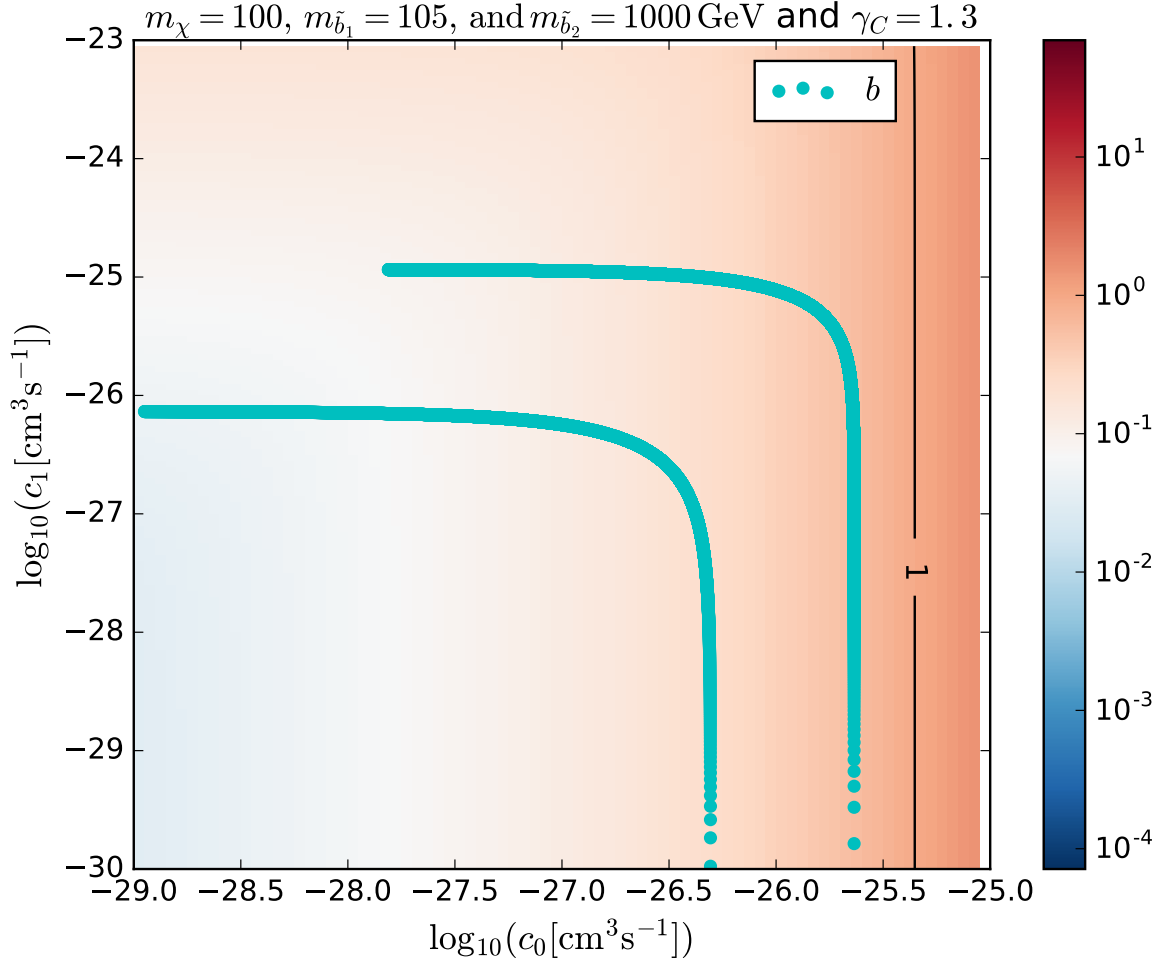


**Figure 9. Depleted spike, Simplified model plot, scan over mixing angle  $\alpha$ :** The green points correspond to a scan over the mediator mixing angle  $\alpha$  defined by Eq. 4.3. The Yukawa couplings are held fixed at their supersymmetric values, given by Eq. 4.4. The DM mass is 100 GeV and the lightest sbottom mass is 105 GeV, with all other superpartners heavy. The annihilation cross section is parametrized by Eq. 3.1. The solid black line denotes the contour of the integrated flux  $\Phi_{Fermi} = 2.18 \times 10^{-8}$  photons/cm<sup>2</sup>s, coming from the source 3FGL J1745.6-2859c (Sgr A\*), assuming an energy range of 1-100 GeV and  $b\bar{b}$  final states in DM annihilation. The spike profile is given by Eq. 2.3. The spike radius is given by the **depleted** case in Eq. 2.10, with a value  $r_{sp} \sim 0.004$  pc. The spike power law outside the spike radius is given by  $\gamma_c = 1.3$ . The spike power law inside the spike radius is given by Eq. 2.16, yielding  $\gamma_{sp} \sim 2.37$ .

consider consists of bino DM with mass  $m_\chi = 100$  GeV, the lightest bottom squark with mass  $m_{\tilde{b}} = 105$  GeV, and all other superpartners heavy. The solid black line denotes the contour of the integrated flux  $\Phi_{Fermi} = 2.18 \times 10^{-8}$  photons/cm<sup>2</sup>s.

As in the case of the previous figures, we can see from the depleted case with  $\gamma_c = 1.3$

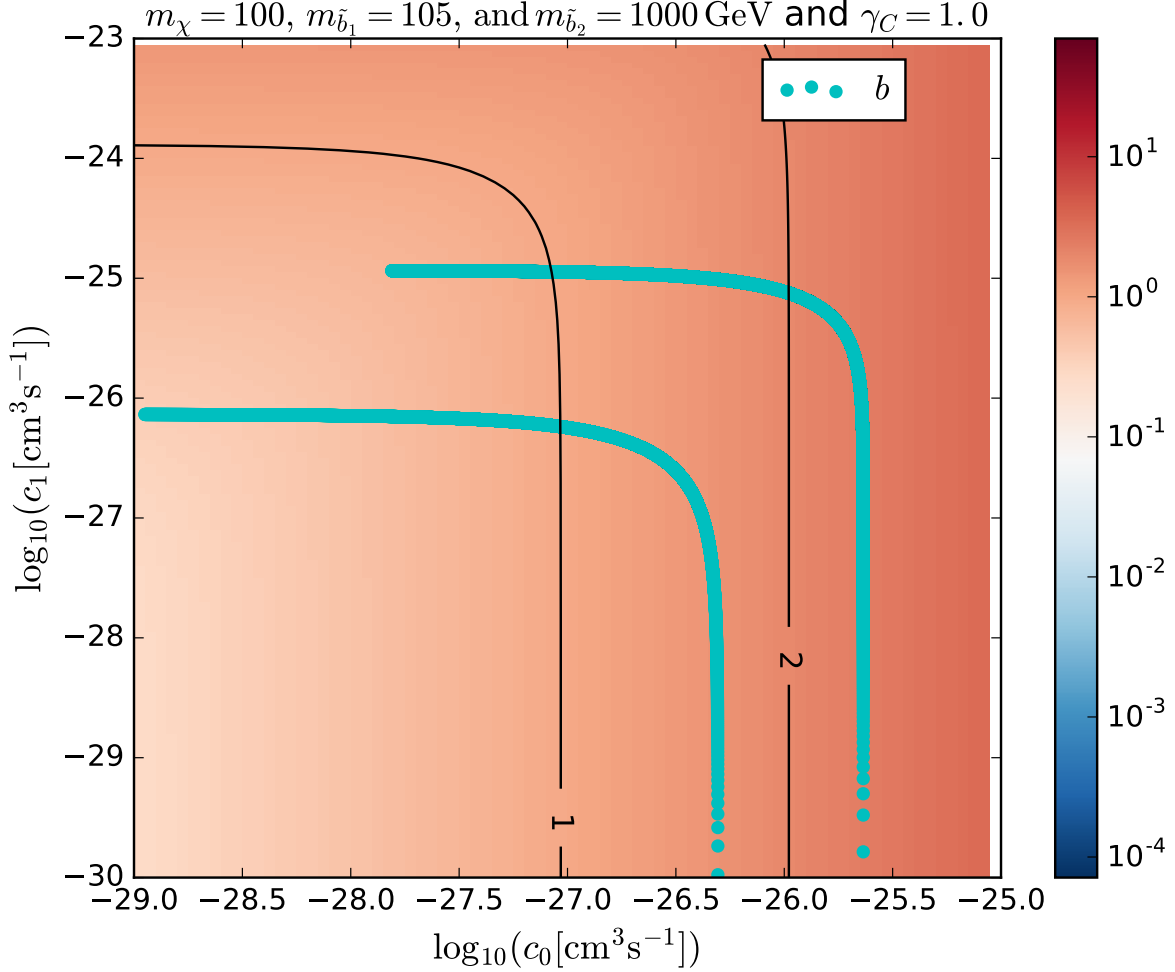


**Figure 10. Idealized spike, Simplified model plot, scan over mixing angle  $\alpha$ :** The green points correspond to a scan over the mediator mixing angle  $\alpha$  defined by Eq. 4.3. The Yukawa couplings are held fixed at their supersymmetric values, given by Eq. 4.4. The DM mass is 100 GeV and the lightest sbottom mass is 105 GeV, with all other superpartners heavy. The annihilation cross section is parametrized by Eq. 3.1. The solid black line denotes the contour of the integrated flux  $\Phi_{Fermi} = 2.18 \times 10^{-8}$  photons/cm<sup>2</sup>s, coming from the source 3FGL J1745.6-2859c (Sgr A\*), assuming an energy range of 1-100 GeV and  $b\bar{b}$  final states in DM annihilation. The spike profile is given by Eq. 2.3. The spike radius is given by the **idealized** case in Eq. 2.8, with  $r_{sp} = 0.40$  pc. The spike power law outside the spike radius is given by  $\gamma_c = 1.0$ . The spike power law inside the spike radius is given by Eq. 2.16, yielding  $\gamma_{sp} \sim 2.33$ .

considered in Fig. 12, that current observational constraints just barely begin to constrain the parameter space. The constraints are much stronger for the case of an idealized spike in Fig. 13 where even for  $\gamma_c = 1.0$ , the current observational limits constrain a large part of the

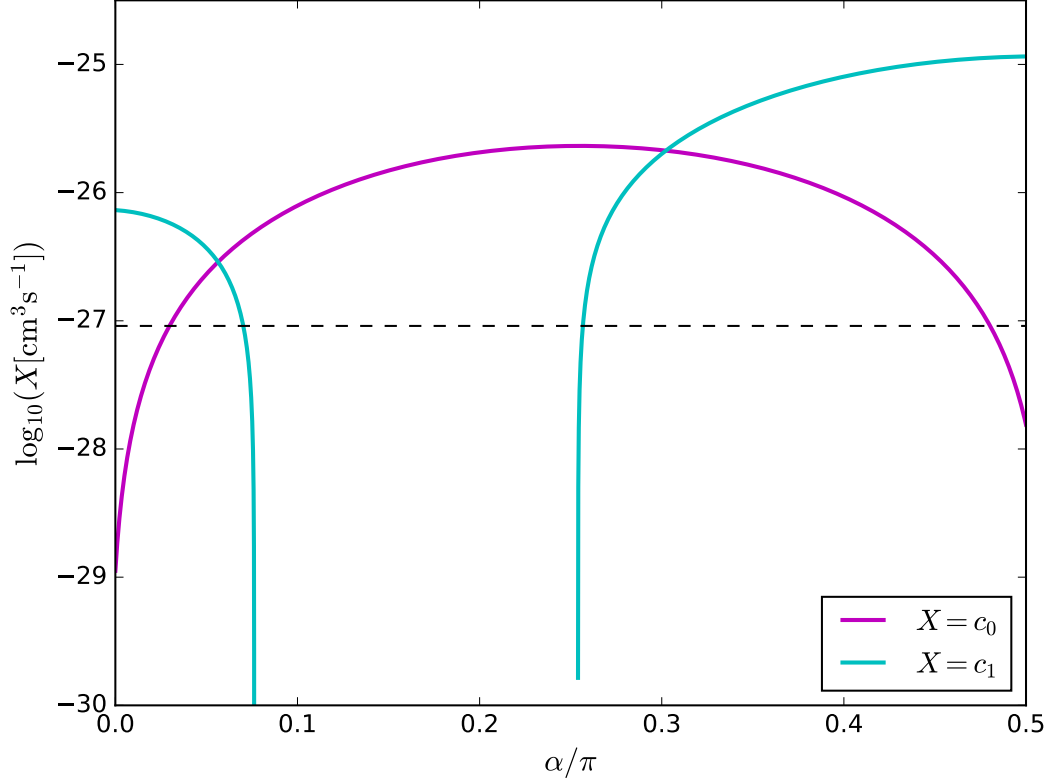


**Figure 11. Dependence of  $c_0$  and  $c_1$  on  $\alpha$ :** The purple and blue curves show the dependence of  $c_0$  and  $c_1$  on  $\alpha$  as obtained from Eq. 4.8 and Eq. 4.9, respectively. The horizontal dotted line corresponds to the contour  $\Phi = \Phi_{Fermi}$  from Fig. 10 (idealized spike with  $\gamma_c = 1.0$ ). Values of  $c_0$  above the dotted line are constrained by the integrated flux of photons coming from the source 3FGL J1745.6-2859c (Sgr A\*).

parameter space. We find from Fig. 13 that

$$Y_L \cdot Y_R > 0.084 \quad (4.11)$$

is constrained by the gamma-ray flux.

## 5 Constraints on Spike Parameters from DM Annihilations

In this Section, we invert the approach we have hitherto taken. We calculate the constraints on the spike parameters in our model, assuming that the excess of  $\sim 1 - 3$  GeV gamma-rays from the Galactic Center observed by Fermi-LAT is due to DM annihilations. We calculate

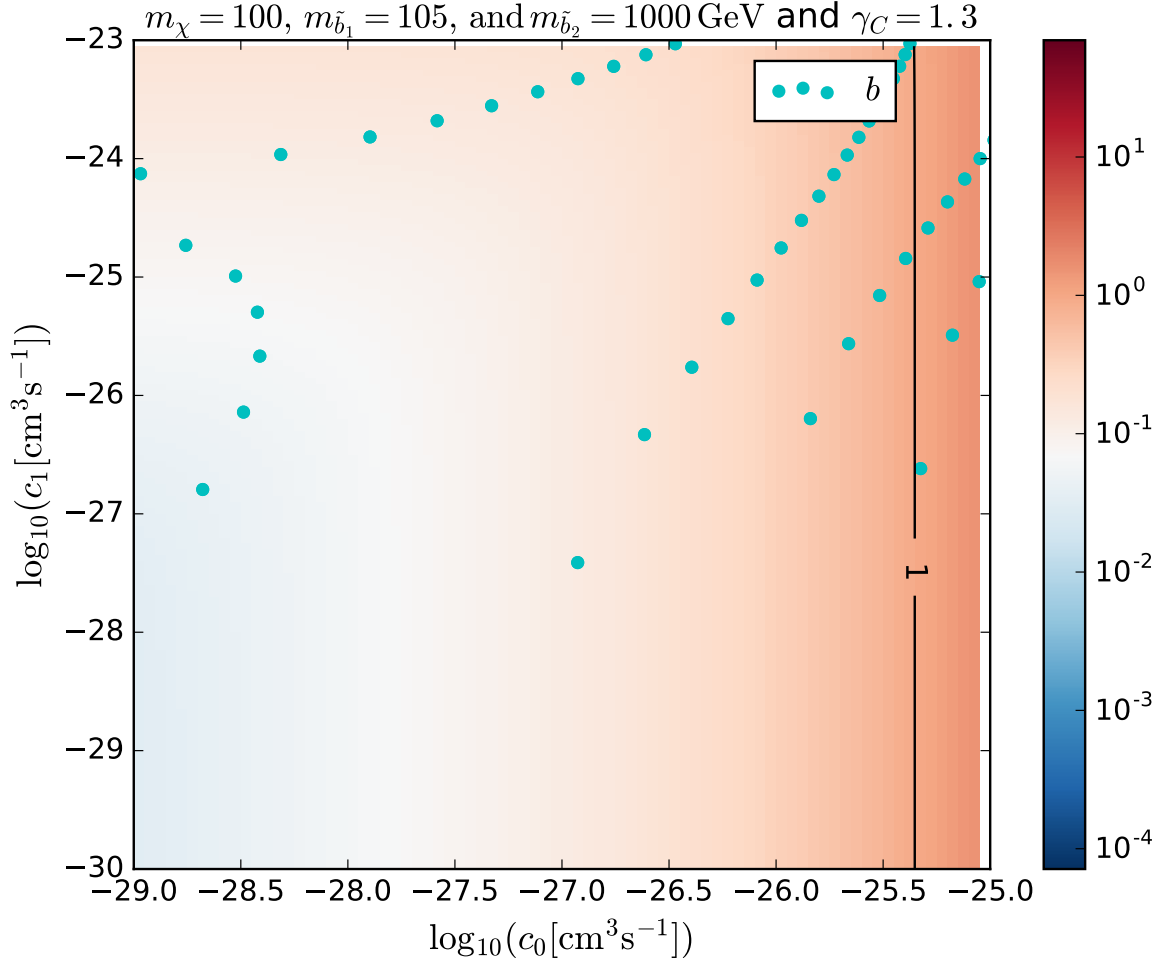


**Figure 12. Depleted spike, Simplified model plot, scan over Yukawa couplings  $\lambda_{L,R}$ :** The green points correspond to a scan over the Yukawa couplings defined by Eq. 4.2, in the range 0 to  $\sqrt{4\pi}$ . The DM mass is 100 GeV and the lightest sbottom mass is 105 GeV, with all other superpartners heavy. The annihilation cross section is parametrized by Eq. 3.1. The solid black line denotes the contour of the integrated flux  $\Phi_{Fermi} = 2.18 \times 10^{-8}$  photons/cm<sup>2</sup>s, coming from the source 3FGL J1745.6-2859c (Sgr A\*), assuming an energy range of 1-100 GeV and  $b\bar{b}$  final states in DM annihilation. The spike profile is given by Eq. 2.3. The spike radius is given by the **depleted** case in Eq. 2.10, with a value  $r_{sp} \sim 0.004$  pc. The spike power law outside the spike radius is given by  $\gamma_c = 1.3$ . The spike power law inside the spike radius is given by Eq. 2.16, yielding  $\gamma_{sp} \sim 2.37$ .

the gamma-ray flux from the DM spike in our model, taking as a benchmark point

$$\begin{aligned}
 m_\chi &= 49 \text{ GeV}, \\
 c_0 &= 1.76 \times 10^{-26} \text{ cm}^3 \text{ s}^{-1} \\
 c_1 &= 1.0 \times 10^{-30} \text{ cm}^3 \text{ s}^{-1}
 \end{aligned} \tag{5.1}$$

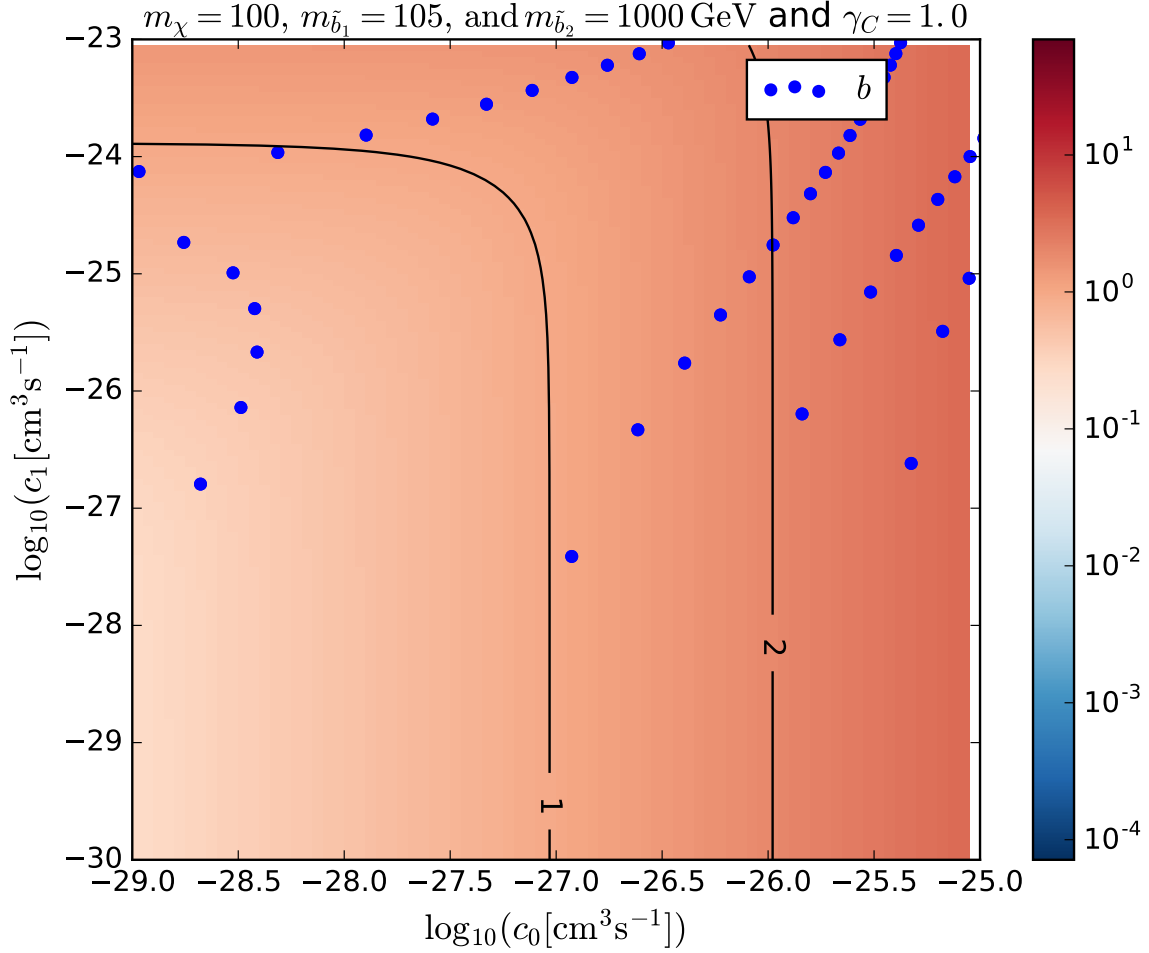


**Figure 13. Idealized spike, Simplified model plot, scan over Yukawa couplings  $\lambda_{L,R}$ :** The green points correspond to a scan over the Yukawa couplings defined by Eq. 4.2, in the range 0 to  $\sqrt{4\pi}$ . The DM mass is 100 GeV and the lightest sbottom mass is 105 GeV, with all other superpartners heavy. The annihilation cross section is parametrized by Eq. 3.1. The solid black line denotes the contour of the integrated flux  $\Phi_{Fermi} = 2.18 \times 10^{-8}$  photons/cm<sup>2</sup>s, coming from the source 3FGL J1745.6-2859c (Sgr A\*), assuming an energy range of 1-100 GeV and  $b\bar{b}$  final states in DM annihilation. The spike profile is given by Eq. 2.3. The spike radius is given by the **idealized** case in Eq. 2.8, with  $r_{sp} = 0.40$  pc. The spike power law outside the spike radius is given by  $\gamma_c = 1.0$ . The spike power law inside the spike radius is given by Eq. 2.16, yielding  $\gamma_{sp} \sim 2.33$ .

and assuming  $b\bar{b}$  final states, as in [32].

Clearly, many choices for the spike parameters exist, and considering different combinations would lead to different kinds of constraints on the parameter space. As a representative case, we consider the case of a depleted spike and put constraints on the  $\gamma_{sp}$  vs.  $\gamma_c$  plane. The spike radius is given by the depleted case in Eq. 2.10, with values  $r_{sp} \sim 0.002 - 0.046$



pc.

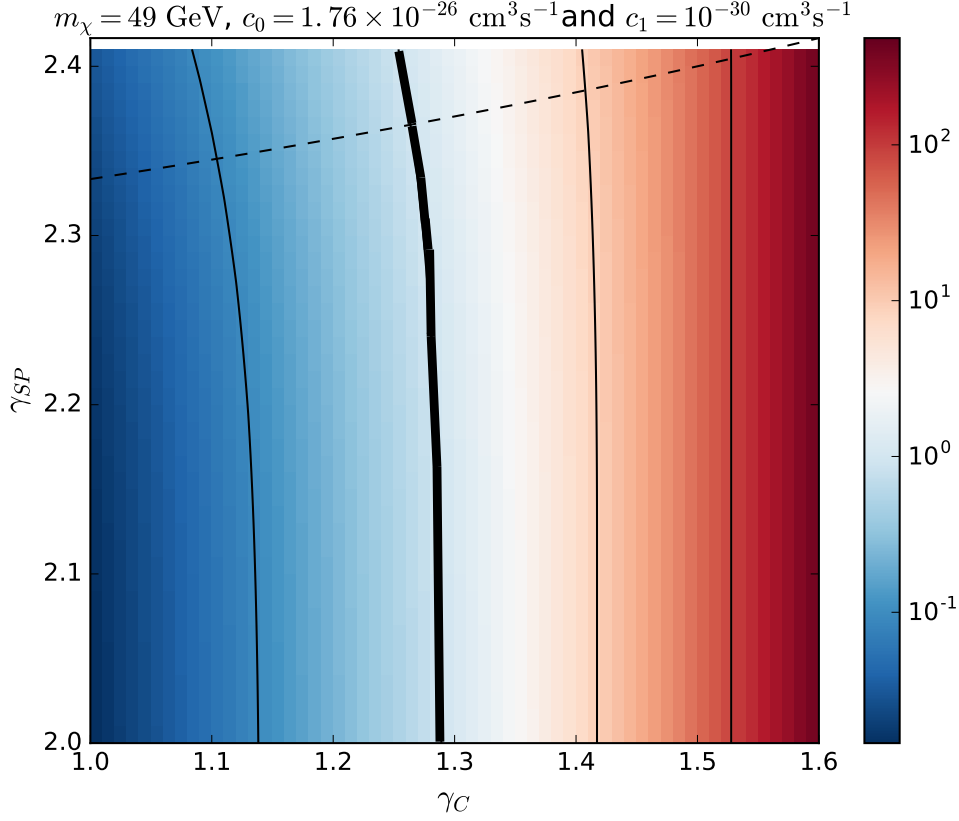


**Figure 14. Constraints on Spike Parameters, assuming Depleted Spike and GC Excess:** The DM mass is 49 GeV and the annihilation cross section is parametrized by Eq. 3.1, with  $c_0 = 1.76 \times 10^{-26} \text{ cm}^3 \text{ s}^{-1}$  and  $c_1 = 1.0 \times 10^{-30} \text{ cm}^3 \text{ s}^{-1}$ . The solid black contours denote the integrated flux  $\Phi$  in units of  $\Phi_{Fermi} = 2.18 \times 10^{-8} \text{ photons/cm}^2 \text{ s}$  coming from the source 3FGL J1745.6-2859c (Sgr A\*), assuming an energy range of 1-100 GeV and  $b\bar{b}$  final states in DM annihilation. The bold contour corresponds to  $\Phi = \Phi_{Fermi}$ . The spike profile is given by Eq. 2.3. The spike radius is given by the depleted case in Eq. 2.10, with values  $r_{sp} \sim 0.002 - 0.046 \text{ pc}$ . The dotted line shows the relation between  $\gamma_{sp}$  and  $\gamma_c$  given by Eq. 2.16.

The results are displayed in Fig. 14. The solid black contours denote the integrated flux  $\Phi$  in units of  $\Phi_{Fermi} = 2.18 \times 10^{-8} \text{ photons/cm}^2 \text{ s}$  coming from the source 3FGL J1745.6-2859c (Sgr A\*), assuming an energy range of 1-100 GeV. The dotted line shows the relation between  $\gamma_{sp}$  and  $\gamma_c$  given by Eq. 2.16. It is clear that for our choice of spike profile, values of  $\gamma_c \gtrsim 1.3$  are incompatible with a DM interpretation of the Galactic Center excess for most values of  $\gamma_{sp}$ .

In Fig. 15, we display the constraints on a DM candidate satisfying the conditions in Eq. 5.1. The contours denote the cases where the integrated flux  $\Phi = \Phi_{Fermi} = 2.18 \times$

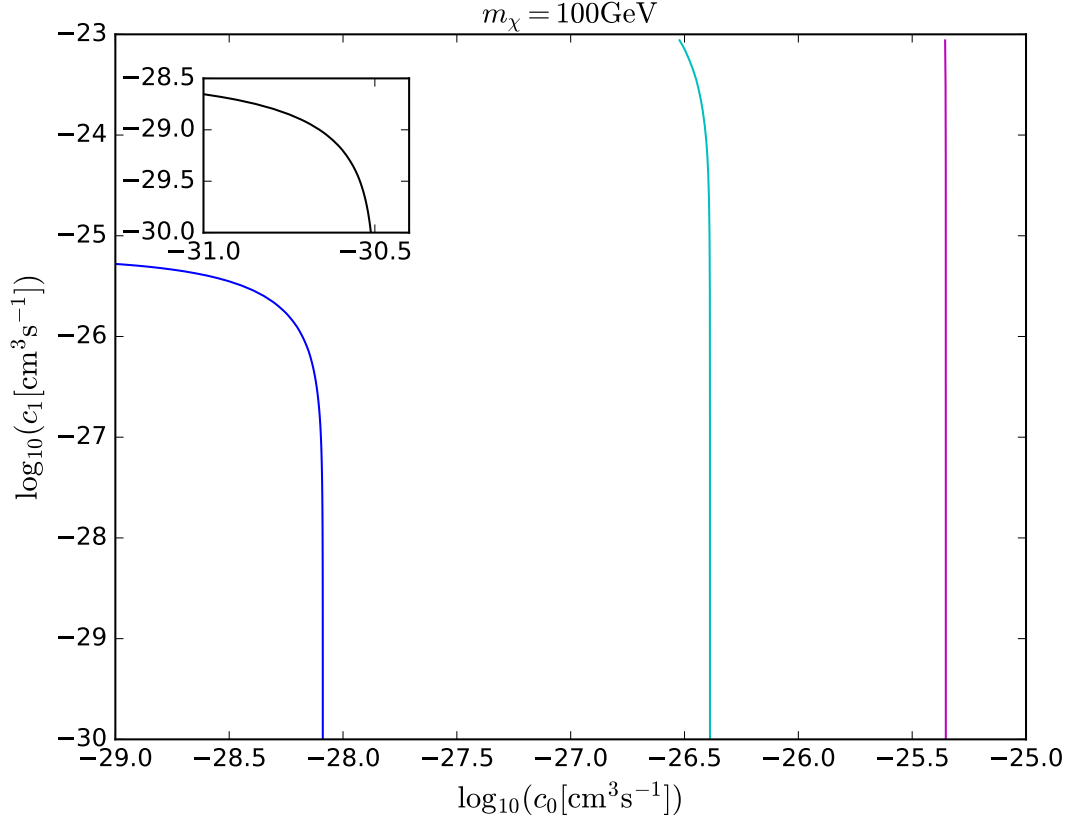


**Figure 15. Constraints on DM:** The DM mass is 49 GeV and the annihilation cross section is parametrized by Eq. 3.1. The contours denote the cases where the integrated flux  $\Phi = \Phi_{Fermi} = 2.18 \times 10^{-8}$  photons/cm<sup>2</sup>s coming from the source 3FGL J1745.6-2859c (Sgr A\*), assuming an energy range of 1-100 GeV and  $b\bar{b}$  final states in DM annihilation. The spike profile is given by Eq. 2.3. The spike radius is given by the depleted case in Eq. 2.10, with values  $r_{sp} \sim 0.002 - 0.046$  pc. The magenta, cyan, and blue contours correspond to  $\gamma_c = 1.3, 1.4, 1.5$ , respectively. The inset shows the contour corresponding to  $\gamma_c = 1.6$ .

$10^{-8}$  photons/cm<sup>2</sup>s. The magenta, cyan, and blue contours correspond to  $\gamma_c = 1.3, 1.4, 1.5$ , respectively. The inset shows the contour corresponding to  $\gamma_c = 1.6$ .

## 6 Conclusions

In this paper, we have studied contributions of a DM spike near the central black hole of our Galaxy to the gamma-ray flux  $\Phi$ . As our reference gamma-ray source, we have taken 3FGL J1745.6-2859c (Sgr A\*) from Fermi-LAT's Third Point Source Catalog. We have taken into account a variety of astrophysical parameters describing the spike, and calculated the resulting constraints on general models of DM. We have then taken these constraints and applied them

to a specific simplified model of fermionic DM with  $t$ -channel mediators. Finally, we have inverted our approach and considered the case of a DM candidate fitting the Galactic Center excess, and calculated the resulting constraints on the space of astrophysical spike parameters.

We have found that the spike formation history and profile parameters have a profound effect on the extent to which models of DM can be constrained.

(i) For the most conservative choice of parameters (a depleted spike with radius given by Eq. depletion,  $\gamma_c = 1.0$ ), the flux for a 100 GeV thermal relic is several order of magnitude below current observational limits. We have then considered a series of less conservative choices.

(ii) A depleted spike with steeper cusp profile can constrain thermal relics of different masses depending on  $\gamma_c$ , as shown in Fig. 5. We see that thermal relics, approximately of masses 15 GeV, 50 GeV, and 140 GeV, are constrained by the choice of spike profile and different selections of  $\gamma_c = 1.3, 1.4$ , and 1.5, respectively.

(iii) An idealized spike which has not undergone attenuation improves the results considerably; the mass reach is shown in Fig. 6. This assumes that the inner spike profile corresponds to a scenario where the DM spike formed in response to the adiabatic growth of the black hole, i.e.,  $\gamma_{sp} \sim 2.3 - 2.4$ . We see that thermal relics, approximately of masses 25 GeV, 80 GeV, and 240 GeV, are constrained by the choice of spike profile and different selections of  $\gamma_c = 1.0, 1.1$ , and 1.2, respectively.

(iv) Relaxing the assumption of an adiabatic growth of the black hole results in less steep spike profiles; for a particular choice of smoother profile  $\gamma_{sp} = 1.8$ , the mass reach is shown in Fig. 7. We see that thermal relics, approximately of masses 15 GeV, 50 GeV, and 140 GeV, are constrained by the choice of spike profile and different selections of  $\gamma_c = 1.2, 1.3$ , and 1.4, respectively.

We have then gone on to apply these results for the simplified model of fermionic DM with  $t$ -channel mediators described by Eq. 4.1. In particular, we have performed scans over the mixing angle  $\alpha$  and the Yukawa couplings of the theory, and checked to what extent the models are constrained by the observational limits of the gamma-ray flux from 3FGL J1745.6-2859c (Sgr A\*). We have found that while a depleted spike radius just barely begins to constrain the parameter space, an idealized spike constrains large parts of it, even for the most conservative choice of the cusp profile  $\gamma_c = 1.0$ .

Finally, we have placed constraints on the space of astrophysical spike parameters, assuming that the Galactic Center excess is due to DM annihilations. We have taken a representative case of a depleted spike, and found that values of  $\gamma_c > 1.3$  are incompatible with a DM interpretation of the Galactic Center excess for most values of  $\gamma_{sp}$ .

## 7 Acknowledgement

We would like to thank Mustafa Amin for collaboration in the early stages of this work. PS is supported in part by NSF Grant No. PHY-1417367.

## References

- [1] R. Genzel *et al.*, *Astrophys. J.* **594**, 812 (2003) [arXiv:astro-ph/0305423].
- [2] R. Schodel, T. Ott, R. Genzel, A. Eckart, N. Mouawad and T. Alexander, *Astrophys. J.* **596**, 1015 (1971) [arXiv:astro-ph/0306214].
- [3] P. Gondolo and J. Silk, “Dark matter annihilation at the galactic center,” *Phys. Rev. Lett.* **83**, 1719 (1999) [arXiv:astro-ph/9906391].
- [4] P. Ullio, H. Zhao and M. Kamionkowski, “A Dark-Matter Spike at the Galactic Center?,” *Phys. Rev. D* **64**, 043504 (2001) [arXiv:astro-ph/0101481].
- [5] D. Merritt, *Phys. Rev. Lett.* **92**, 201304 (2004) [arXiv:astro-ph/0311594].
- [6] G. Bertone and D. Merritt, “Time-dependent models for dark matter at the Galactic center,” *Phys. Rev. D* **72**, 103502 (2005) [arXiv:astro-ph/0501555].
- [7] O. Y. Gnedin and J. R. Primack, *Phys. Rev. Lett.* **93**, 061302 (2004) doi:10.1103/PhysRevLett.93.061302 [astro-ph/0308385].
- [8] E. J. Ahn, G. Bertone and D. Merritt, *Phys. Rev. D* **76**, 023517 (2007) doi:10.1103/PhysRevD.76.023517 [astro-ph/0703236 [ASTRO-PH]].
- [9] F. Acero *et al.* [Fermi-LAT Collaboration], *Astrophys. J. Suppl.* **218**, no. 2, 23 (2015) doi:10.1088/0067-0049/218/2/23 [arXiv:1501.02003 [astro-ph.HE]].
- [10] B. D. Fields, S. L. Shapiro and J. Shelton, *Phys. Rev. Lett.* **113**, 151302 (2014) doi:10.1103/PhysRevLett.113.151302 [arXiv:1406.4856 [astro-ph.HE]].
- [11] J. Shelton, S. L. Shapiro and B. D. Fields, *Phys. Rev. Lett.* **115**, no. 23, 231302 (2015) doi:10.1103/PhysRevLett.115.231302 [arXiv:1506.04143 [astro-ph.HE]].
- [12] S. L. Shapiro and J. Shelton, *Phys. Rev. D* **93**, no. 12, 123510 (2016) doi:10.1103/PhysRevD.93.123510 [arXiv:1606.01248 [astro-ph.HE]].
- [13] M. A. Amin and T. Wizansky, *Phys. Rev. D* **77**, 123510 (2008) doi:10.1103/PhysRevD.77.123510 [arXiv:0710.5517 [astro-ph]].
- [14] P. Sandick and S. Watson, *Phys. Rev. D* **84**, 023507 (2011) doi:10.1103/PhysRevD.84.023507 [arXiv:1102.2897 [astro-ph.CO]].
- [15] P. Sandick, J. Diemand, K. Freese and D. Spolyar, *PoS IDM* **2010**, 086 (2011) [arXiv:1012.0068 [astro-ph.CO]].
- [16] P. Sandick, J. Diemand, K. Freese and D. Spolyar, *JCAP* **1101**, 018 (2011) doi:10.1088/1475-7516/2011/01/018 [arXiv:1008.3552 [astro-ph.CO]].
- [17] D. Schoonenberg, J. Gaskins, G. Bertone and J. Diemand, *JCAP* **1605**, no. 05, 028 (2016) doi:10.1088/1475-7516/2016/05/028 [arXiv:1601.06781 [astro-ph.HE]].
- [18] M. Wanders, G. Bertone, M. Volonteri and C. Weniger, *JCAP* **1504**, no. 04, 004 (2015) doi:10.1088/1475-7516/2015/04/004 [arXiv:1409.5797 [astro-ph.HE]].
- [19] M. Garny, A. Ibarra and S. Vogl, *Int. J. Mod. Phys. D* **24**, no. 07, 1530019 (2015) doi:10.1142/S0218271815300190 [arXiv:1503.01500 [hep-ph]].

- [20] P. Sandick, K. Sinha and F. Teng, JHEP **1610**, 018 (2016) doi:10.1007/JHEP10(2016)018 [arXiv:1608.00642 [hep-ph]].
- [21] J. Kumar, P. Sandick, F. Teng and T. Yamamoto, Phys. Rev. D **94**, no. 1, 015022 (2016) doi:10.1103/PhysRevD.94.015022 [arXiv:1605.03224 [hep-ph]].
- [22] K. Fukushima, C. Kelso, J. Kumar, P. Sandick and T. Yamamoto, Phys. Rev. D **90**, no. 9, 095007 (2014) doi:10.1103/PhysRevD.90.095007 [arXiv:1406.4903 [hep-ph]]; K. Fukushima and J. Kumar, Phys. Rev. D **88**, no. 5, 056017 (2013) doi:10.1103/PhysRevD.88.056017 [arXiv:1307.7120 [hep-ph]].
- [23] G. Bertone and D. Merritt, Mod. Phys. Lett. A **20**, 1021 (2005) doi:10.1142/S0217732305017391 [astro-ph/0504422].
- [24] L. Ferrarese and H. Ford, Space Sci. Rev. **116**, 523 (2005) doi:10.1007/s11214-005-3947-6 [astro-ph/0411247].
- [25] J. Diemand, M. Kuhlen, P. Madau, M. Zemp, B. Moore, D. Potter and J. Stadel, Nature **454**, 735 (2008) doi:10.1038/nature07153 [arXiv:0805.1244 [astro-ph]].
- [26] J. F. Navarro *et al.*, Mon. Not. Roy. Astron. Soc. **402**, 21 (2010) doi:10.1111/j.1365-2966.2009.15878.x [arXiv:0810.1522 [astro-ph]].
- [27] O. Y. Gnedin, A. V. Kravtsov, A. A. Klypin and D. Nagai, Astrophys. J. **616**, 16 (2004) doi:10.1086/424914 [astro-ph/0406247].
- [28] M. Gustafsson, M. Fairbairn and J. Sommer-Larsen, Phys. Rev. D **74**, 123522 (2006) doi:10.1103/PhysRevD.74.123522 [astro-ph/0608634].
- [29] M. Pato, F. Iocco and G. Bertone, JCAP **1512**, no. 12, 001 (2015) doi:10.1088/1475-7516/2015/12/001 [arXiv:1504.06324 [astro-ph.GA]].
- [30] E. Vasiliev, Phys. Rev. D **76**, 103532 (2007) doi:10.1103/PhysRevD.76.103532 [arXiv:0707.3334 [astro-ph]].
- [31] T. Sjostrand, S. Mrenna and P. Z. Skands, JHEP **0605**, 026 (2006) doi:10.1088/1126-6708/2006/05/026 [hep-ph/0603175].
- [32] T. Daylan, D. P. Finkbeiner, D. Hooper, T. Linden, S. K. N. Portillo, N. L. Rodd and T. R. Slatyer, Phys. Dark Univ. **12**, 1 (2016) doi:10.1016/j.dark.2015.12.005 [arXiv:1402.6703 [astro-ph.HE]]; F. Calore, I. Cholis and C. Weniger, JCAP **1503**, 038 (2015) doi:10.1088/1475-7516/2015/03/038 [arXiv:1409.0042 [astro-ph.CO]]; D. Hooper, JCAP doi:10.1016/j.dark.2016.11.005 [arXiv:1608.00003 [astro-ph.HE]].